• U C •
FCTUC FACULDADE DE CIÊNCIAS
E TECNOLOGIA
UNIVERSIDADE DE COIMBRA

UNWARPING HEATED BONES

A Quantitative Analysis of Heat-induced Skeletal Deformations Using 3D Geometric Morphometrics

Ficha Técnica:

Tipo de trabalho	**Dissertação de Mestrado**
Título	**UNWARPING HEATED BONES: A Quantitative Analysis of Heat-induced Skeletal Deformations Using 3D Geometric Morphometrics**
Autor	**João Pedro Valente de Oliveira Coelho**
Orientadora	**Professora Doutora Eugénia Cunha**
Coorientador	**Doutor David Miguel da Silveira Gonçalves**
Identificação do Curso	**Mestrado em Evolução e Biologia Humanas**
Área científica	**Biologia**
Especialidade/Ramo	**Antropologia Biológica**
Data	**2015**

ACKNOWLEDGMENTS

Getting here would be impossible without the contribution of people to whom I am greatly indebted. I shall attempt to do them justice with words.

First of all, I greet my advisors, Professor PhD Eugénia Cunha and PhD David Gonçalves for all the support, guidance and important advices. By giving me this opportunity and believing in me you've truly contributed to my growth as an individual.

Although not officially on paper, there is someone I consider a mentor as well. Thank you PhD Francisco Curate for trusting in this project from the very start.

There are two research groups that have welcomed me: CIAS and the Laboratory of Forensic Anthropology. If I felt welcomed in these 'temples' is also due to PhD Vitor Matos, Professor PhD Ana Luísa Santos, PhD Luciana Sianto, PhD Luis Marado, PhD Maria Teresa Ferreira, MD Samantha Wijerathna, Catarina Coelho, Amanda Hale and Débora Pinto. Thank you all for the help, company and moments of brainstorming. This goes twofold to David Navega, who helped troubleshooting programming issues many times while being a first-rate pal *like they do in the future*.

To my dear colleagues from the HOT Project, Calil Makhoul, Inês Santos, Márcia Gouveia and Ana Vassalo, what I've said in the previous paragraph also applies to you. I'm very grateful to share a spot with you all in this team. Also, I take the chance to recognize again David Gonçalves. What you are aiming at is grand and wonderful. I wish all the success for this project and everyone related to it.

To my comrades Filipe Monteiro, Daniela Cunha and Cláudia Fernandes, thanks for the companionship, inspiration and motivation. *Osteomics starts now*!

It goes without saying that I feel grateful to all the teachers, colleagues and friends I've met in Coimbra and Reykjavík. I hold very dear all the mentorship, knowledge and great moments you gave me during this 5 years of academic life.

Last but not least, to all my friends, dear family and Carolina: thanks for the friendship, unconditional support, and Love. I am here for you. All you got to do is ask.

João Pedro Valente de Oliveira Coelho

ABSTRACT

Human burnt remains are a tremendous challenge for bioanthropologists. In the case of skeletons, due to the extensive and chaotic transformations bones and teeth undergo throughout heat-transfer, methods for estimating the biological profile are biased if applicable. Many attempts have been successful in improving techniques, mainly in accessing sex, although there is still much room for improvement. Two particularly problematic heat-induced changes that undermine trust in traditional osteometric methods are skeletal shrinking and warping.

In the present framework these two observable occurrences have been reinterpreted as size and shape changes, respectively. Despite seeming a quite simple intuition, it allows theoretical reformulation of the problem at hand. Bearing in mind that quantitative estimation, interpretation and comparison of size and shape in anatomical entities are issues that have already been solved by the Geometric Morphometrics Synthesis.

Given the advantage of current statistical shape analysis approaches outlined in the previous paragraph, it is quite remarkable that no previous instances of researching burnt remains from such perspective were found in the literature. Therefore, this preliminary study is the first of its kind and it already showed some potential for the creation of predictive models relevant for the forensic sciences.

It was demonstrated that combining Geometric Morphometrics and Machine Learning is a very promising route for shape analysis of heat-altered osteological material. By applying Logistic Model Trees on the Relative Warps of Procrustes Shape coordinates, the maximum temperature at which a bone was burnt was predicted with an overall accuracy of 82%. Multivariate regression in the context of Procrustes ANOVA also shows promise to regress bone shape by using only a few variables. However, caution should be taken with the provided results: sample size is quite small, and a comprehensive validation is yet to be done.

Keywords: burnt remains, retrodeformation, warping, shrinking, shape analysis

RESUMO

Restos humanos queimados representam um desafio interpretativo para os bioantropólogos. No caso do esqueleto, devido às extensas e caóticas transformações que os ossos e os dentes sofrem por transferência de calor, os métodos para estimativa do perfil biológico, caso aplicáveis, tendem a ser enviesados. Têm havido esforços em prol dos avanços metodológicos, particularmente em estimativa do sexo, contudo muito permanece por fazer. O encolhimento e o arqueamento ósseos induzidos pelo calor são dos principais impedimentos ao uso dos métodos osteométricos tradicionais.

Estes dois fenómenos observáveis foram aqui reinterpretados como sendo modificações de tamanho e forma, respectivamente. Apesar desta intuição parecer simplista, permite uma reformulação teórica do problema presente. Visto que a análise quantitativa e comparativa do tamanho e da forma em entidades anatómicas são questões que foram resolvidas pela Síntese Morfométrica.

Considerando as vantagens da abordagem acima referida, é notável não terem sido encontradas referências na literatura de restos esqueléticos queimados utilizando por base os métodos da morfometria geométrica. Portanto, este estudo preliminar é o primeiro do seu género e já apresenta ter algum potencial para a criação de modelos preditivos com relevância para as ciências forense.

Demonstrou-se que o combinar da morfometria geométrica com métodos computacionais de aprendizagem automatizada traduz-se numa abordagem muito promissora para a análise da forma em material osteológico termicamente alterado. Ao aplicar um *Logistic Model Trees* em componentes principais das coordenadas de Procrustes, obteve-se um modelo capaz de prever a temperatura máxima da queima do osso com uma exatidão de 82%. Utilizou-se técnicas de regressão multivariada dentro do contexto comparativo de uma ANOVA de Procrustes, o que pode vir a ter algum potencial para regredir a forma a partir de um pequeno conjunto de variáveis. Contudo, cautela é indispensável com os resultados obtidos: o tamanho da amostra ainda é reduzido e é necessário realizar validação dos resultados com outra amostra similar.

Palavras-chaves: ossos queimados, retrodeformação, arqueamento, encolhimento, análise da forma

TABLE OF CONTENTS

INDEX OF TABLES

INDEX OF FIGURES

LIST OF ABBREVIATIONS

ML	Machine Learning
GMM	Geometric Morphometrics methods
CEI/XXI	21st Century Identified Skeletal Collection
CS	Centroid Size
$\boldsymbol{\rho}$	Procrustes distance
$\boldsymbol{d_F}$	Full Procrustes distance
$\boldsymbol{d_p}$	Partial Procrustes distance
p	Number of landmarks in a shape matrix
k	Number of dimensions in a shape matrix
m	Number of individuals in a shape matrix
n	Sample size
TPS	Thin-Plate Spline
LMT	Logistic Model Trees
PCA	Principal Components Analysis

1 INTRODUCTION

1.1 MOTIVATION AND AIMS

> "Insofar as here the element required to *heat* the machine seems to be the same element as is to be investigated by means of the machine"
> — (Nietzsche, [1878–1880] 1996: 321)

Forensic anthropologists attempt to narrow down the missing person list by tracing biological profiles of skeletons from a plethora of complex contexts (Dirkmaat et al., 2008). In order to accomplish such endeavor, the current paradigm focus on estimation of age-at-death (Cunha et al., 2009), sex (Bruzek & Murail, 2006), ancestry (Navega et al., 2014) and stature (Willey, 2014). All these share the fact that they can be assessed, within some expected error, through osteometric or morphoscopic aspects. However, when bones or teeth have been in contact with heat at high temperatures during some period of time, morphology might become severely deformed (Randolph-Quinney, 2014a,b). Therefore, morphometric-based methods created through reference collections of unburnt bones are compromised for heat-altered skeletal material (Fairgrieve, 2007; Gonçalves et al., 2013).

Currently, partial skeletons are being subjected to high temperatures and then curated within the 21st Century Identified Skeletal Collection housed at the University of Coimbra (Ferreira et al., 2014). Benefiting from such experimental setting, a theoretical leverage for developing new robust methodologies in heat-altered osteology is within grasp. In order to accomplish that, privileged access to data on pre-burning and post-burning circumstances has to be transformed into useful models with the ability to estimate conditions that the anthropologist cannot accurately guess in the field, such as maximum temperature or even original shape of the heat-altered bone. By training Machine Learning (ML) models with morphological and contextual data attained before, during and after the heating experiment, the aim is to directly address the current bias in osteometric estimations provoked by the quite complex and seemingly chaotic heat-induced changes in shape and size.

For doing so, a logic and cohesive scheme of specific objectives have been integrated, and can be summarized as follows:

1. To digitally curate 3D meshes of the sampled osteological material
    a. Before these are thermally modified (since these will be altered forever);
    b. After these are thermally modified (because of its fragile and brittle state);
    c. Create an accessible virtual database of comparable material.
2. Understand the potential of 3D Geometric Morphometrics to
    a. Compare visually and statistically, how heat changes bones;
    b. Recreate the bone original form (i.e. virtual retrodeformation);
    c. Measure objectively the **warping** *phenomenon*;
    d. Quantify differences in size, and so, measure **shrinkage** objectively.
3. Perform data analysis to access
    a. If the experimental design strategy is undergoing a proper direction;
    b. The ability to create new predictive models to estimate
        i. Non-shape variables from shape-variables;
        ii. Shape variables from non-shape variables.

It is expected that if accomplished together, our goals might promote new solutions to target the problem of not being able to know or correctly estimate the form a bone had previously to being burned. That is indeed the hidden element one wishes to investigate and that can only be retrieved through duteous data collection in controlled experimentation. Auspiciously, not only was that condition fully met, but also ended up droving all the analytical components of the current dissertation.

Heretofore, was Nietzsche ([1878–1880] 1996) envisioning something akin to ML when reflecting on the *Duty for Truth* problematic? Maybe, or the similarity is purely coincidental, as he was abstracting a conceptual mind and its respective obligation to search for reason. That is pretty much what scientists working in Artificial Intelligence are aspiring to accomplish. Nonetheless, his aphorism strikingly applies: *Insofar as here the unaltered and heat-altered shapes are required to be fed into a pattern recognition algorithm as to understand morphological heat-alterations by means of the trained algorithm*. Major difference being that *heat* is now being used literally instead of figuratively, as understanding its effects on skeletons are what drive this dissertation.

1.2 HEAT-INDUCED SKELETAL CHANGES: STATE-OF-THE-ART

> "Of course first-hand experimentation, when feasible, is the perfect answer to the question, *How did this happen*?"
>
> — (DeHaan, 2015: 14)

Across the various phases of the heating process, bones get severely altered in many morphological and structural aspects. These include fragmentation, chromatic modification, weight loss, fracturing, and size and shape deformations (Ubelaker, 2009; Randolph-Quinney, 2014b). Taken together, these might be helpful for forensic reconstruction of the circumstances related to the fire event, cremation or heating experiment (McKinley, 2000). For example, macroscopic appearance of the various colors that can show up in osteological material have been regarded as clues of a bone's biochemical conditions and the environmental context associated with a specific burning process (Shipman et al., 1984; Mayne-Correia, 1997).

Likewise, heat-induced fractures have been studied extensively, particularly thumbnail fractures. The last have been associated with gradual exposition of wet bone surface during heating as the protective tissue contracts (Symes et al., 2013, 2015). However, this fails to explain why thumbnail fractures appear in dry bones (Gonçalves et al., 2014). As an alternative explanation Gonçalves et al. (2011) suggested thumbnail fractures can be associated with collagen preservation. Other fractures have also been linked to pre-burning osteological conditions, and a concise but thorough review is available by Gonçalves (2012).

Unfortunately, the just described aspects of heat-induced changes, such as color changes and fractures, cannot be, at least in any clear way, analytically studied with the chosen theoretical approach. In this research, a macromorphologic approach based on a systematic analysis of tridimensional geometrical properties was employed. Thus, only heat-induced size and shape alterations are focused of this thesis.

Van Vark (1974, 1975) who was an early pioneer on applying multivariate statistics to cremated bones for sex estimation, identifies the changes that bone suffers in size and shape as one of the main difficulties in applying inferential statistics to burnt remains. A solution based on Geometric Morphometrics methods (GMM) will be

presented in order to address this problem. However, before attempting such endeavor, one must 'clean the room' and address issues related to terminology.

Despite many words being thrown in literature to describe shape and size changes promoted by heat-transfer (i.e. twisting, bending, torsion, deformation, volume reduction, dimensional changes, etc.), we will avoid the confusion here by splitting any intrinsic geometric *phenomena* into two distinct types: warping and shrinking. Even though these probably have related causes, we take a step further and define both as fully independent geometric properties of heat-induced changes in order to study them quantitatively. Thus, for our purposes we can define these as:

Warping: all heat-induced **shape change** in anatomical structures.

Shrinking: all heat-induced **size reduction** in anatomical structures.

A validated theory that explains the fundamentals of heat-induced bone warping (Figure 1-1) is yet to be found (Gonçalves et al., 2014). Four different hypothesis that attempt to address the fundamental cause of warping have been proposed: (1) due to contraction of muscle fibers (Binford, 1963); (2) triggered by heat trapped in the shaft hollow (Spennemann & Colley, 1989); (3) anisotropic distribution of bone collagen results into differential periosteum contraction, thus warping the bone (Thompson, 2005); (4) completes the former by adding that the degree of warping might be dependent on collagen-apatite bonds preservation (Gonçalves et al., 2011). Notice that the earliest do not address the problematic of observing warping in bone without protective tissues. The first ever way to objectively quantify the degree of warping via simple mathematical procedures will be demonstrated later on. It should be emphasized that having such variable might show innovative promise for testing hypothesis as those just mentioned.

As for shrinking (Figure 1-2), research in the 90s have pushed forward robust methodologies to study it quantitatively (Grupe & Hummel, 1991; Nelson, 1992; Holden et al., 1995a,b; Huxley & Kósa, 1999). However these were all focused on microscopic features, rather than gross structure. While microscopy might be the most fruitful way to understand the fundamental basis of bone shrinking (Thompson, 2009), such studies disregarded reaching direct quantification of the full or macromorphological shrinking.

Figure 1-1 - Heat-induced warping illustrated with CEI/XXI 65. This *phenomena* can be described as a bowing or an arching of the bone in the sense that it deforms the relative position of the epiphysis in respect to the centroid. Left we have a virtual layered comparison of pre-burnt (40% opacity) versus post-burnt (80% opacity). In center we have the right humerus that was burnt at 900°C for 116 minutes. For comparison, in the right we have the left humerus that was not burnt of the same individual. This bone also shows evident fractures and shrinking.

Thus, it becomes a hard task to establish correlations, or to create predictive models of the shrinking *phenomenon*. Some authors (Thompson, 2005; Gonçalves et al., 2013) have been successful in estimating gross anatomical shrinkage, unfortunately through reduced Euclidean measurements. Reduced, in the sense that bidimensional distances do not match the geometrical definition of size, even if there is a correlation among size and arbitrary lengths and widths. Overall, traditional morphometry has major statistical issues and theoretical problems that have been covered by Zelditch et al. (2012). Just to give an example, all measures in a structure tend to be highly correlated among them, meaning there are very few independent variables despite many measurements.

Although it has been observed that size alterations can behave very differently (even presenting expansion sometimes) along the same anatomical entity, through measuring different metrics across the same bone (Thompson, 2005), that might be possibly due to using traditional measuring such as lengths and widths to evaluate size, instead of landmark-defined configurations. Since in this thesis, bone shrinking was defined as being exclusively related to size (i.e. shape-independent), any particular difference in sub-anatomic areas are forcefully shape-related and therefore are considered to be warping instead of shrinking. Mixing the two hinders any objective measurement of either, at least through any available mathematics as of today. Accordingly, non-tridimensional measurements (i.e. lengths, widths, ratios, angles, surface areas, etc.) are biased to address the problem at hand, and a full geometric approach is preferred to quantify size changes. Afterwards, such approach shall be demonstrated as well through an elegant mathematical formulation.

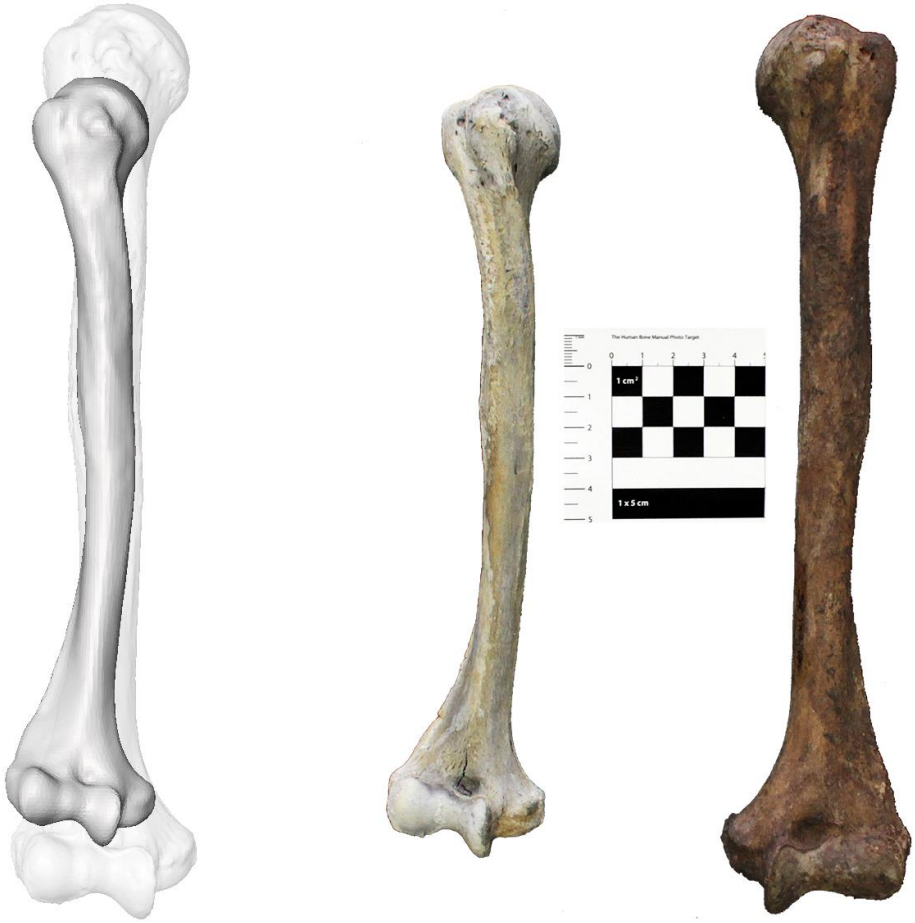

Figure 1-2 - Heat-induced shrinking illustrated with CEI/XXI 35. This individual was chosen because it had the 2nd highest shrinking value, despite having relatively low warping (6th lowest in the sample). Left we have a virtual layered comparison of pre-burnt (40% opacity) and post-burnt (80% opacity). In center we have the right humerus that was burnt at 900°C for 150 minutes. In the right we have the left humerus that was not burnt (for comparison).

1.3 TERMINOLOGY OF A GEOMETRIC APPROACH: A REVIEW

"What's in a name? that which we call a rose
By any other name would smell as sweet"
— (Shakespear, [1597] 1993: II.ii:47)

Now that it was clarified which heat-induced skeletal changes are of interest, it is important to define terms concerning statistical analysis of morphological entities. Since these have concrete mathematical definitions and should not be confused with the vernacular way in which most are thrown around in day-to-day speech.

1.3.1 WHAT FORMS SHAPE AND SHAPES FORM? A MATTER OF SIZE

During the last 30 years, morphometricians synthetized powerful analytical tools from non-Euclidean Geometry, Matrix Algebra and Multivariate Statistics into a single framework and that would not be possible with ill-defined terminology. Most of the following definitions are crucial for understanding GMM and were adapted from the masterworks of Dryden & Mardia (1998) and Zelditch et al. (2012).

Geometric Morphometrics: an algebraic approach that transforms problems from morphology into problems of geometry, allowing for a toolbox of analytical tools to be applicable onto anatomical landmarks.

Landmark: a point of correspondence on each entity that matches between and within populations (*e.g.* the *Nasion* in *crania*).

Shape: all the geometric information remaining in a set of landmarks after differences in location, scale and rotational effects are removed.

Size: Any positive real valued function g(X), such that g(A**X**) = Ag(**X**), where **X** is a matrix of points and A is any positive, real scalar value. The size measure or the A favored in GMM is Centroid Size (see definition below).

Form: all the geometric information remaining in a set of landmarks after differences in location and rotational effects are removed. Thus, form is similar to shape, except that it preserves scale. Form is also been referred to as size-and-shape, since it is a combination of both concepts.

Centroid Size: A measure of geometric scale, calculated as the square root of the summed squared distances of each landmark from the centroid of the landmark configuration. It is favored as a size measure, because it is uncorrelated with shape in the absence of allometry, and also because Centroid Size (*CS*) is congruent with the definition of Procrustes distance (see below). For a given matrix **X**, the Centroid Size is acquired by

$$CS(\mathbf{X}) = \sqrt{\sum_{i=1}^{p}\sum_{j=1}^{k}\left(\mathrm{X}_{ij} - \mathrm{C}_{j}\right)^{2}} \qquad (1)$$

where the sum is over the rows i and columns j of the matrix **X**. Thus, X_{ij} specifies the component located on the i^{th} row and j^{th} column of the matrix **X** and C_j stands for the location of the j^{th} value of the centroid. This formula is generalized for p landmarks on k dimensions.

Procrustes distance (ρ): is the sum of squared distances between corresponding points of two superimposed shapes. When the shape being superimposed is reduced in Centroid Size to minimize further the difference between it and the target, the distance may be called a *Full Procrustes distance* (d_F). When both sizes are held at centroid size = 1, the distance may be called a *Partial Procrustes distance* (d_P). Depending on the anteceding algebraic transformations, any of the presented *Procrustes distances* types between two individuals **A** and **B** can be mathematically defined as

$$\rho(\mathbf{A}, \mathbf{B}) = \sqrt{\sum_{i=1}^{p}\sum_{j=1}^{k}\left(\mathrm{A}_{ij} - \mathrm{B}_{ij}\right)^2} \qquad (2)$$

where the sum is over the squared result of subtracting rows *i* and columns *j* of the matrix **A** to the analogous *i* and *j* of matrix **B**. Hence, X_{ij} and W_{ij} specify the component located on the i^{th} row and j^{th} column of the **X** and **W** matrices. These sums are generalized for *p* landmarks on *k* dimensions.

1.3.2 LANDMARKS: MAPPING ANATOMY THROUGH GEOMETRY

Knowing which landmarks should be documented in any anatomical structure depends on the hypothesis being tested or the general objectives of a study. Selecting a coherent configuration of anatomical points is perhaps the single most important step in any shape analysis. Thus is useful to understand the difference between types (Figure 1-3) as well as their statistical proprieties and assumptions (Dryden & Mardia, 1998). Within GMM there are 3 classic types of landmarks, here we adapt definitions provided in the Glossary of Zelditch et al. (2012) and originally settled by Bookstein (1997a,b).

Type 1 landmarks: Defined in terms of local information, such as the junction of three bones or two bones and a muscle. With Type 1 there is no need to refer to any distant structures or relative positions.

Type 2 landmarks: Defined by a relatively local property, such as the maximum or minimum of curvature of a small bulge or at the endpoint of a structure. It is considered less useful than Type 1 landmarks because the evidence for their homology is possibly geometric rather than biological.

Type 3 landmarks: Regarded as deficient because they have one less degree of freedom than they have coordinates, which is lost when specifying how to locate

the landmark. These can be used in a statistical shape analysis, but the loss of a degree of freedom must be taken into account when performing inferential tests.

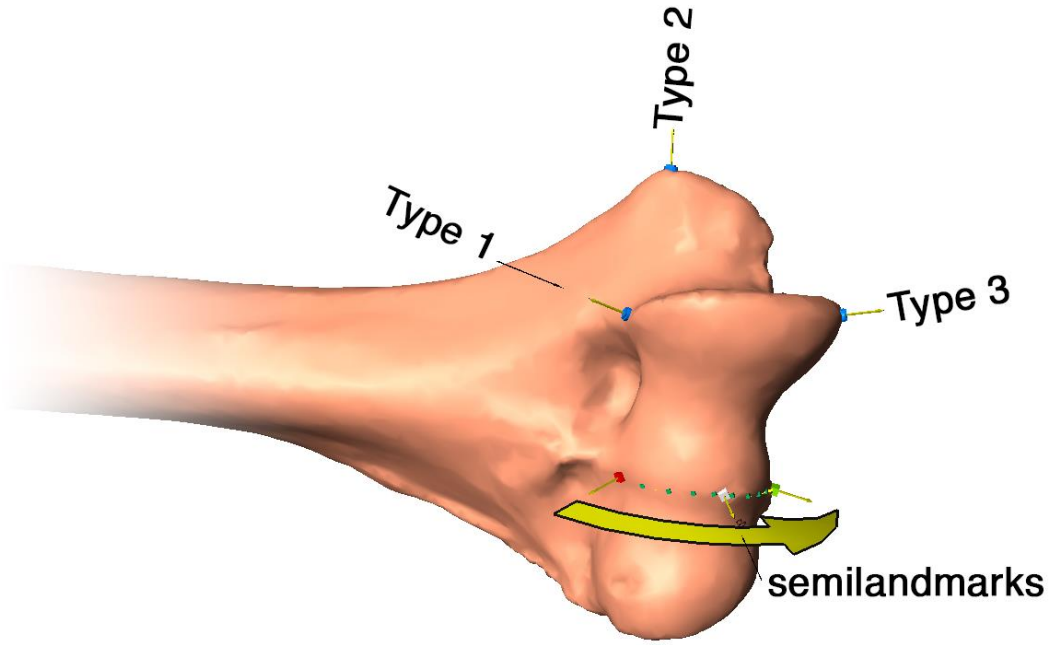

Figure 1-3 - Main types of landmarks illustrated with the distal part of CEI/XXI 26 right humerus (before heating experiment). Examples are: the proximal anterior point of the medial trochlea (Type 1); the most projecting point of the medial epicondyle (Type 2); Middle curvature point of the medial trochlea (Type 3). There are also 10 semilandmarks defining the curvature of the lateral trochlea (yellow arrow represents their order within the shape matrix). A descriptive list of selected landmarks for my data analysis can be found at Appendix 6.1.

It is also important to describe here two additional types of landmarks. It might seem at first that these are avoiding the logic of well-defined biological homology. However their intent is roughly the same and their usefulness comes from the innovative possibilities they offer. First, semilandmarks are defined, which are known for having many diverse and interesting applications and achieved popularity and drastic theoretical improvements during the last years (Gunz & Mitteroecker, 2013). Next, a description of pseudolandmarks is provided, following Boyer et al. (2015). With pseudolandmarks the 'homology' is definitely geometric in its essence, but they are particularly important for employing automated landmark acquisition techniques through computational means (Coelho et al., 2015):

Semilandmarks: Used to integrate information about curvature, these are points in curves, edges or surfaces, defined in terms of relative position within aforesaid features (*e.g.* at 90% of the length of the sagittal crest). Because semilandmarks are

not discrete anatomical *loci* and require to be defined through other features, they contain fewer degrees of freedom than landmarks, hence the "semi-".

Pseudolandmarks: Computer-placed landmarks. All the individuals have to be defined by the same number of points, as in observer-placed landmarks. Aiming to provide each coordinate with a fairly consistent biological identity across the sample, without human intervention. Their definition does not fit the criteria of either of the 3 types of landmarks (Zelditch et al., 2012), neither semilandmarks (Mitteroecker & Gunz, 2009; Gunz & Mitteroecker, 2013).

1.4 GEOMETRIC MORPHOMETRICS MEETS BURNT REMAINS THEORY

"Yet, that is precisely what the theory of shape demands of us; if we do not think of the problem in terms of whole landmark configurations, we will be led to theoretically invalid solutions."

— (Zelditch et al., 2012: 404)

As far as it has been inferred from the research into literature, GMM were never been applied to study the shape of thermally modified skeletal material. Consequently, this is unmapped territory and must be approached prudently. Bearing in mind that the initial steps are only now being taken, the first thing to point out is this study can only ever attempt at being exploratory. However there are already some general negative and positive points from using this approach with burnt skeletal remains that can be described.

A cautionary note is that GMM can never become an optimal solution for solving all morphological problems with burnt remains. A major problem of this approach is that when heat-induced bone fragmentation is severe, it might be impossible to define a sufficient number of landmarks. Unfortunately, this could represent the majority of the scenarios an osteologist has to deal. Furthermore, if one includes burnt material from archaeological contexts into this consideration (Whyte, 2001). While current methodologies for estimating missing landmarks are quite robust, these clearly add some

bias to the sample. The problem here is that there are already too many factors increasing statistical noise, and there is no need to take the risk of bringing an extra one if it happens to affect the majority of the sample.

Within the most important insights obtained from introducing GMM into the field of burnt human osteology, are the new ways of measuring important aspects of heat-induced changes that have been exposed. First, that shape distances such as the *Full Procrustes distance* can give an easily reproducible quantitative estimate of heat-induced skeletal warping. This is useful since warping tends to be recorded by a scoring binary system (i.e. present *versus* absent, *e.g.* Gonçalves et al., 2014) or through artificially created categorical ranks. Next, that by subtracting a reference Centroid Size from a bone after it was subjected to heat, to the *CS* value of the same bone before the heating experiment, it is also possible to estimate the amount of size change a bone has undergone, thus effectively estimating heat-induced skeletal shrinking. Even if the term shrinkage was preferred here to describe the process, if the value obtained is negative it would rather be indicative of expansion, which according to Thompson (2005) might happen as well. Under the Laws of Thermodynamics it is expectable that objects dilate when exposed to heat and thus it is not that impressive to obtain such results with heat-altered bones.

It is hoped that these intuitions will be incorporated into the field of burnt remains osteology and ultimately contribute to pursuing new avenues for testing hypothesis that have remained untestable for too long, or were tested until now mostly through very indirect or subjective metrics.

2 MATERIALS AND METHODS

2.1 MATERIALS

> "To find out what happens to a system when you interfere with it you have to interfere with it (not just passively observe it)."
>
> — (Box, 1966: 629)

The sample was comprised of 20 individuals from the 21st Century Identified Skeletal Collection (herein CEI/XXI, after its original name in Portuguese: *Colecção de Esqueletos Identificados do Século XXI*), which is housed at the Laboratory of Forensic Anthropology, in the Life Sciences Department of the University of Coimbra (Ferreira et al., 2014). More precisely, this sample belonged to a subgroup of skeletons from within the aforesaid collection that were partially burned under experimental conditions using an electric muffle-furnace with thermostat (Gonçalves et al., 2015).

2.1.1 CEI/XXI

As a new collection it is remarkable that CEI/XXI, as of now, already has over 200 complete skeletons of recently deceased individuals. Quite *sui generis* in its composition, it is of striking importance for the current scene in European forensic anthropology (Ferreira et al., 2014) and shows noteworthy potential for providing insights into the bioanthropology of contemporary populations (Curate, 2011). All the skeletons are from individuals inhumed at the *Capuchos* graveyard located in Santarém, Portugal. These were unclaimed by relatives and thus donated to the University of Coimbra.

To understand the relevance of CEI/XXI it is better lo look at some descriptive statistics and population parameters. Currently the collection is composed by 113 females and 89 males, so a total n = 204 skeletonized individuals. The range of age-at-death for females is 38 to 100 years, with mean = 81.35, sd = 12.447 and median = 84. Male individuals have died younger, as can be perceived by the min-max = [27-95[, mean =

72.33 and median = 77. Which is an expected well-known worldwide trend known as the mortality gender-gap (Rogers et al., 2010). Also, the male sample is more spread out with a standard deviation of 17.057. It is thus a collection with a strong geriatric component with potential to bring insight into some extremely complicated issues, such as age-at-death estimation in adults. Currently there is not a precise enough method for estimation of age-at-death in advanced phases of life (Cunha et al., 2009).

2.1.2 HOT PROJECT

Within the CEI/XXI collection some selected skeletons are being partially burned under laboratorial conditions. Consequently, a sub-collection that currently counts with 20 partially burnt individuals is undergoing development. For summary description, the age-at-death in the current sample ranges from 70 to 90 years old (mean = 80.26, sd = 6.31), and sex representation is quite balanced (11 females and 9 males). It is also worth remarking that only bones with bilateral antimeres are being burnt. Henceforth the other side is kept for comparison and future research (Makhoul et al., 2015). The general steps of the protocol used during the controlled heating experiment are briefly illustrated in Figure 2-1.

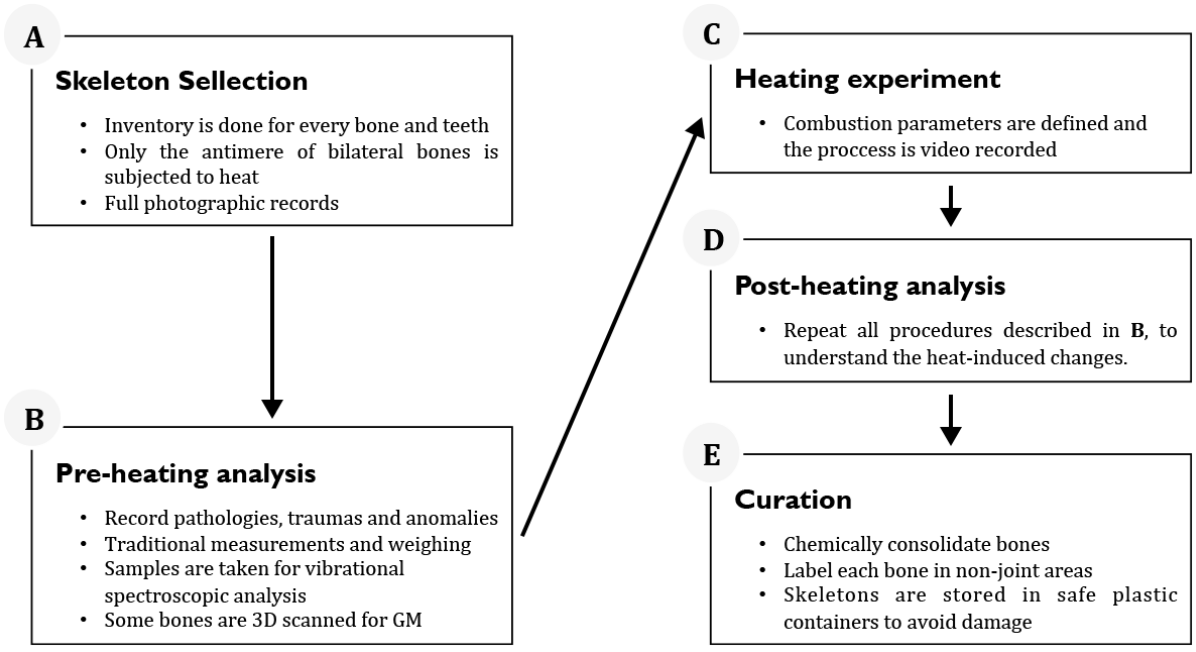

Figure 2-1 - Brief summary of the HOT Project Protocol. The aim is to minimize error, since many researchers are involved and to maximize preservation, because the burnt bones might be useful for future research (adapted from

Makhoul et al., 2015). For more information the reader should visit the site of the project at http://hotresearch.wix.com/main

It is expected that this collection will improve the current state of knowledge on heat-induced changes in human bones and teeth and also to upgrade current, or create new analytical methods that could be useful for researchers of burnt skeletal remains. This could promote methodological improvement in forensic anthropology of arson crimes (Thompson, 2005), fire-related disasters (Gonçalves et al., 2015) and bioarchaeology of cremated remains and funerary rituals (Gonçalves et al., 2011).

There were some drawbacks on using data from the HOT Project for extrapolations that could be truly useful in real-word forensic scenarios. For example, the 20 individuals from this dataset were all buried for a minimum of 70 months and therefore did not tend to have any soft tissue attached. Differing from dealing with burnt bodies in a forensic setting, where not having soft tissues prior to burning is rarely the case. For reviews of the effects of heat in soft tissues check Payne-James et al. (2003) and Saukko & Knight (2004). Another possible problem that was not being accounted for was the position or the way a bone lies in the muffle during burning. Because gravitational effects and the changes in the relative position of the center of mass during the heating experiment might affect the way a bone deforms. The team is currently testing how influent this problem is and hopefully insights will arise about its impact in the near future and how it should be experimentally controlled.

Despite limitations, being able to work with heat-altered human skeletons under laboratorial conditions already represents considerable progress when compared to research that used instead faunal remains in their experimental designs (*e.g.* Spennemann & Colley, 1989; Whyte, 2001; Thompson, 2005; Munro et al., 2007). At least when considering direct applicability of the acquired knowledge into real cases in forensic anthropology or bioanthropology.

2.2 MESH ACQUISITION AND GEOMETRIC SAMPLE SIZE

In order to apply GMM to any dataset of tridimensional anatomical structures there are usually three options: (1) to directly obtain Cartesian coordinates through a high-precision 3D digitizer such as MicroScribe; (2) to use medical imaging techniques

(*e.g.* CT, MRI, etc.) to acquire full volumetric information; or (3) to get polygonal meshes of the anatomy through surface laser scanning. For this dissertation, the last approach was preferred and applied to all the *humeri* of the individuals in our sample. The humerus was selected because of its relevance in biological profiling, and also since it displays quite representatively the range of possible heat-induced alterations in long bones without becoming excessively fragile.

In a first phase, the *humeri* of our 20 individuals were virtually reconstructed through NextEngine™ 3D Scanner HD and its associated software ScanStudio™ HD (NextEngine™, 2015). Following, an open-source 3D mesh processing system, MeshLab, was used to create a watertight 3D model (Cignoni et al., 2008). This procedure to obtain virtual 3D representations of the *humeri* was repeated after the heating experiment. In a geometrical sense and in terms of statistical modeling this duplicated the total sample size (n = 40). However, one humerus was not possible to scan before heating (individual **CEI/XXI 77**), and even though data about it was collected, this individual was not used in the shape statistical analysis, **reducing our effective *n* to 19** (geometric n = 38, since its post-burning mesh was also discarded). This was not seen as a major problem, since the individual 77 was an outlier to begin with. As it was burnt at only 500 degrees Celsius (i.e. the lowest temperature in the sample) and despite the striking dark coloration and a 31% mass reduction (also the lowest, sample mean = 39.32%), there were no noticeable form deformations in the humerus and no evidences of calcination, in other words it has only undergone carbonization.

2.2.1 3D LASER SCANNING STRATEGY

The pipeline for tridimensional laser scanning of long bones was designed, based on suggestions and protocols first proposed by Filiault (2012). After many trials, a procedure that takes between 30 and 45 minutes to virtually render a complete humerus with high quality was chosen. It should be noted that the long bones from the human body take considerable more time and dedication when considering the limitations of a NextEngine™ (2015). Because of its shape and size, multiple laser scanning in different positions is necessary in order to obtain great detail and successfully align the joint final

mesh. When the bones are calcined, extra care is required, because of the inherent fragility of the osteological material after experimental heat alterations.

Before GMM was thought to be included into the experimental protocol of the HOT Project, already 9 skeletons were subjected to partial burning. Accordingly, we would have a very small sample size, of only 11 individuals. So, the antimeres of the previously burnt *humeri* were also 3D scanned for 8 of those 9 skeletons. Then, these were virtually mirrored, meaning some left *humeri* were transformed into right *humeri* or vice-versa, in order to maximize our *n*.

To perform 3D shape mirroring via computational means, it is necessary to flip one of the axes, while freezing the shape matrix. This was carried out for individuals 24, 29, 32, 49, 50, 57, 64, 65 and 77 of the CEI/XXI collection. However, as already mentioned, it was decided to not use in our analysis the last one that besides being an outlier, its antimere has severe trauma with associated bone growth, plus taphonomic erosion and thus was very asymmetric (Figure 2-2), which would inject unnecessary bias into our sample that would be hard to handle statistically.

Figure 2-2 - *Humeri* of individual CEI/XXI 77. The right humerus (on top) was burnt at 500ºC for 75 minutes. Having considered the trauma in the left humerus' diaphysis, and the taphonomic process in the lateral side of the proximal epiphysis, it was decided to not mirror the left humerus or to even use data from this individual in the final analysis.

2.2.2 MESHLAB: GETTING ANATOMICAL 3D MODELS READY FOR ANALYSIS

Afterwards, post-processing of the 3D meshes is achieved with the help of MeshLab (Cignoni et al., 2008). Since the meshes generated through laser scanning usually possess excess detail and noise, holes, and non-manifold vertices and edges, we need to apply computational techniques such as Poisson Surface Reconstruction (Kazhdan et al., 2006; Kazhdan & Hoppe, 2013). This algorithm uses the distribution of

Poisson as a means of removing many unexpected artifacts that might arise during 3D laser scanning, while being quite effective at closing holes resulting from parts impossible to detect by the laser scanning technology. Thus, an essential step to create watertight tridimensional models (Bolitho et al., 2009; Estellers et al., 2015), which are useful for conceiving automated methods of landmark digitization.

Contemplating the lack of literature in how to generate a 3D virtual anatomical part ready for landmark digitization, attempts were made through trial and error until a protocol that generated reproducible results with consistent quality was developed. It entails the following steps:

1. Load a .ply file (obtained from ScanStudio™ HD) into MeshLab;
2. Remove all non-manifold edges and vertices;
3. Apply Quadric Edge Collapse Decimation:
    a. Reduce to 64000 faces;
    b. Check 'preserve normal';
    c. Check 'preserve topology'.
4. Apply Poisson Surface Reconstruction with the following parameters:
    a. Octree depth: 12;
    b. Solver divide: 6;
    c. Samples per node: 1;
    d. Surface offsetting: 1;
5. Apply Quadric Edge Collapse Decimation to the just created Poisson mesh:
    a. Reduce to 32000 faces;
    b. Check 'preserve normal';
    c. Check 'preserve topology'.
6. Export the final mesh into .off and ASCII .ply formats.

After this procedure, the 3D virtual *humeri* are almost ready for statistical analysis through a group of techniques developed within the Procrustes paradigm for quantitative analysis of shape and form. However, such framework requires the analyst to possess a data matrix with Cartesian coordinates of anatomical landmarks (Bookstein, 1997a,b; Zelditch et al., 2012).

2.3 R: STATISTICAL LANGUAGE

> "Non-reproducible single occurrences are of no significance to science."
> — (Popper, 1959: 66)

All the statistical and morphological analysis was done with R, a free and open source scientific programming language (Claude, 2008; R Core Team, 2015). Choosing this tool was proven to be crucial for the elaboration of this thesis. The main factors influencing the decision of using it were:

- It is multiplatform and works in every OS (Windows, Linux, Apple OS, etc.);
- Dramatically reduces the use of multiple software for morphometric analysis, which increases coherence and reduces compatibility issues (Claude, 2008);
- Statistics done through written code have far bigger reproducibility than when done in point-and-click software (Gandrud, 2013; Stodden, 2015);
- GMM and programming have been going hand-in-hand nearly since the theoretical foundation of the discipline. Popular R packages include geomorph (Adams & Otárola-Castillo, 2013; Adams et al., 2015), shapes (Dryden, 2014), Morpho (Schlager, 2015), Momocs (Bonhomme et al., 2014), among others. These have been created to facilitate the analysis even for non-expert users;
- R has extremely flexible and powerful graphical tools for data visualization (Claude, 2008; Chang, 2012);
- The sheer amount of manuals, scientific and pop-science articles, MOOCs, conferences, workshops, tutorials, online forums, and an ever-growing community of people ready to help make it far more preferable when compared to other extremely specific software with just a handful of users (Horton & Kleinman, 2015).

2.4 LANDMARKS: THE RAW MATERIAL FOR MODERN SHAPE ANALYSIS

2.4.1 AUTO3DGM: AUTOMATIC LANDMARKS IN R

> "This is very beautiful. It is neat, it is modern technology, and it is fast. I am just wondering very seriously about the biological validity of what we are doing with this machine."
>
> — Melvin Moss on using computers for biometrics (*in* Walker et al., 1971: 326)

From an historic point of view, geometric morphometrics tried to answer questions with an inherent biological or evolutionary explanation (Benítez & Püschel, 2014). It had been used consistently as a toolkit to solve problems of phylogeny and taxonomy, modularity and morphological integration, development, allometry, asymmetry, among others (Adams et al., 2013). With that in mind, it is not hard to understand the importance given in the literature to obtain landmarks that are biological homologous between organisms (Zelditch et al., 2012; Claes et al., 2015).

However, here we are not trying to grasp transformations provoked by genetic or developmental constraints, but instead by heat. Also, considering the high number of landmarks that are required to map the complex and chaotic characteristics of bone deformation provoked by heat, automatize landmark acquisition seemed to be a worthwhile option. A package for `R` that fits this purpose has just recently come out, known as `auto3Dgm` (Boyer et al., 2015). Straightaway a preliminary study was done in collaboration with colleagues, using 3D scanned *tali* bones for sex diagnosis. It started as a small project with the aim of learning and testing `auto3Dgm` as a tool for performing geometric morphometric analysis. Eventually, it led to very satisfactory results when using Logistic Model Trees over Procrustes shape matrices and achieved 88% accuracy on sex classification after 10-fold Cross-Validation (Coelho et al., 2015).

Moreover, the automated methods proposed by Boyer et al. (2015), already show results as good or superior as when experts in anatomy manually select the landmarks. Taking everything that has been said to this point, it would seem that using the algorithms provided by Boyer et al. (2015) for automatically acquiring landmarks in a heat deformation problem was theoretically justified.

However, for that to happen substantial numbers of pseudolandmarks need to be acquired. Consequently the digitization process can become too expensive in terms of computational processing power and memory and might be impossible to run it in more modest or older workstations. Unfortunately, the use of `auto3Dgm` for heat-altered bones failed, which might have been caused by lack of computational power available. Or might be simply due to the chaos inherent to heat-deformed bones being just too complex to be understood and perfectly mapped by this particular algorithm.

2.4.2 MANUAL VERSUS AUTOMATIC: A MIDDLE-WAY WINS

Since the fully automatic method of mass-generating pseudolandmarks did not work out, an alternative had to be found. Nevertheless, manually defining landmarks has huge problems: (1) it is too prone to errors; (2) it can become very time-consuming; (3) when a mistake is done, it might become extremely challenging to correct it or even identify it; (4) you have to define all landmarks early on, which needs to be done in a theoretically rigorous way. However there is a semi-automatic approach provided by the software Landmark Editor, where only the 4th problem applies. With this approach it is mandatory to focus on defining all the landmarks prior to the analysis. However, after manually adding them to a first individual that works as a template (a.k.a. 'atlas' in the software's terminology), all other individuals get these landmarks in a more-or-less correct place that the user needs to manually verify and made corrections as it seems anatomically fit, which solves quite easily problems 1, 2 and 3.

In order to select landmarks that would make theoretical sense for my sample, a literature research for well-defined anatomical landmarks of the humerus was done. Chinnery (2004) illustrates complete landmark constellations of post-cranial skeletal elements, including the humerus. Unfortunately the study is about Ceratopsids dinosaurs, and while the landmarks are biological homologous among species it is not that easy to translate the figures into human osteology. On the other hand, Holliday & Friedl (2013) defined landmarks for hominid *humeri*, but unfortunately, with only 19 and a great proportion being either Type II or III landmarks it was considered a suboptimal landmark cluster for us. There are two works by Kranioti et al. (2009) and Tallman (2013) that provide a very good list of landmarks with illustrative definitions, but they only mapped

the epiphyses of the humerus, and understanding the changes in the diaphysis is considered crucial for accomplishing this thesis' objectives. Finally, there is a recent paper by Rosas et al. (2015) that provides incredibly throughout definitions for 43 landmarks of the humerus. Most importantly, since Rosas et al. (2015) had chosen landmarks robust enough to deal with extremely fragmented material (i.e. paleoanthropological *humeri* from Atapuerca), we can safely assume that their approach is also appropriate for shape analysis of heat-deformed bones.

For addressing problems of dimensionality and other non-desirable mathematical proprieties, Type III landmarks from Rosas et al. (2015) were removed. Also if a Type II landmark seemed too hard to obtain or visualize in a virtual 3D environment, it was discarded as well in order to reduce observer error by enhancing reproducibility. Ultimately a protocol with 35 landmarks based on Rosas et al. (2015) protocol was selected to map all the *humeri*'s shapes from our sample (Appendix 6.1).

One last feature of Landmark Editor also worth mentioning is its ability to morphing an anatomical object into another, by controlling the morphing degree through a sidebar. This literally means we can either virtually "burn" or "unburn" a bone controlling how strong the effect of this transformation is (Figure 2-3). This has potential to reconstruct other bones warped by heat even if these do not belong to our original sample, as long as one correctly assigns the same landmarks onto them.

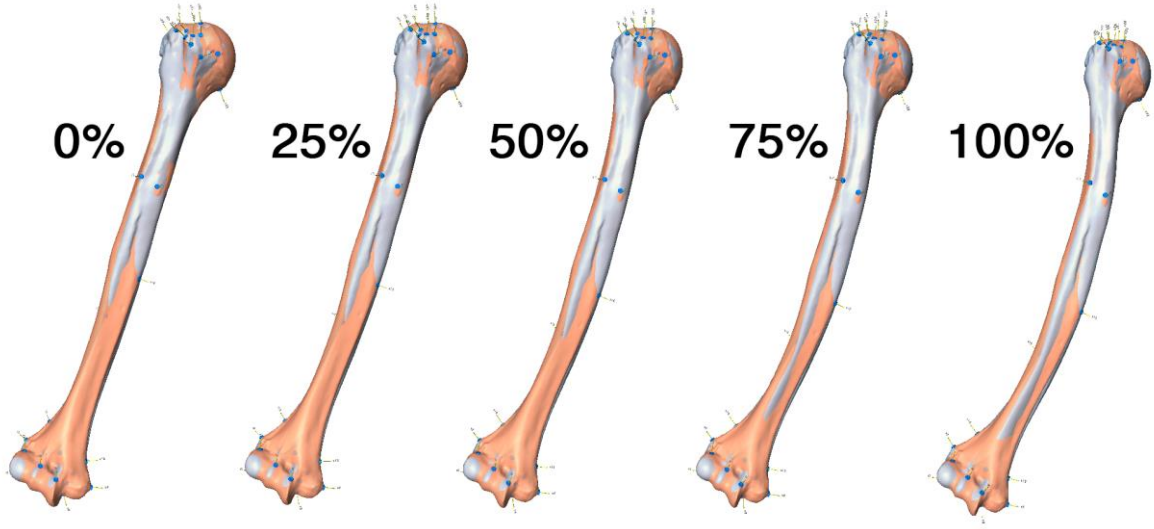

Figure 2-3 - Retrodeformation as a new tool to visually understand warping. Here, the right humerus of the CEI/XXI 5 individual is being morphed from its unburnt to its fully burnt state (900°C for 150 minutes). Orange represents the original unburnt mesh and pale-blue represents where the burnt mesh is dominant. Notice how the pale-blue mesh spreads as the humerus warps. The morphing was broken down into 4 steps, but it could theoretically be broken into infinite steps. Since the models have been scaled to a consensus size, only the effects of warping are being shown, disregarding shrinkage. Otherwise the difference among the 5 stages would be far more evident.

2.5 GEOMORPH: INTEGRATING GEOMETRIC MORPHOMETRICS IN R

After obtaining the landmark configurations for our dataset with the help of Landmark Editor, these are ready for being statistically analyzed. In R, the geomorph package allows the execution of the full workflow of GMM, even though we jumped the first step by doing it in Landmark Editor (an external software, easier to use for this particular part). The full workflow of GMM can be summarized as:

1. Data collection (i.e. landmark digitizing);
2. Data input (i.e. bringing landmark data into R);
3. Data manipulation (i.e. estimating missing values);
4. Generalized Procrustes Analysis (Gower, 1975; Rohlf & Slice, 1990);
5. Data exploration and visualization (Klingenberg, 2013);
6. Data analysis (Mitteroecker & Gunz, 2009).

The two last steps include all the standard techniques of the Geometric Morphometrics toolkit, including Principal Component Analysis (Mitteroecker & Bookstein, 2011), Canonical Variates Analysis (Campbell & Atchley, 1981), Partial Least-Squares (Rohlf & Corti, 2000; Bookstein et al., 2003), Multivariate Regression and Procrustes ANOVA (Zelditch et al., 2012; Adams et al., 2013), Thin-Plate Spline Interpolation (Bookstein, 1989; Green, 1996), among others. For more details on the abilities of the geomorph, check Adams & Otárola-Castillo (2013) and Adams et al. (2015)

The above-mentioned methods allow us to perform statistical analysis of shape variation and its covariation with other variables (Bookstein, 1997a). Moreover, Thin-Plate Spline (TPS) is particularly important, since it can be used to deform a tridimensional shape into another (Gunz & Mitteroecker, 2013). Therefore it has implications for Objective no. 2.b: to reconstruct the original bone shape, before the heat-induced changes have occurred. However it should be noted that the way in which Landmark Editor does this is even easier, and allows partially morphed shapes to be created and saved (thus 3D printable), as well as it has been show previously in Figure 2-3.

2.6 PROCRUSTES SUPERIMPOSITION

> "Shape is all the geometrical information that remains when location, scale and rotational effects are filtered out from an object."
>
> — (Dryden & Mardia, 1998: 1)

Applying Procrustes' algorithms is the contemporary way to obtain insights into morphology and extracting shape information (Rohlf & Slice, 1990; Goodall, 1991; Dryden & Mardia, 1998; Zelditch et al., 2012). This approach is of such ubiquity in Geometric Morphometrics that in a recent review of the state-of-the-art, Adams et al. (2013) dubbed contemporary approaches to statistical analysis of shape as the "Procrustes Paradigm". Generalized Procrustes Analysis (GPA) was first introduced by Gower (1975) as a functional algorithm for removing the effect of position, rotation and size in a set of multiple individuals represented by Cartesian coordinates (Figure 2-4). By discarding this information we obtain a set of consensus shapes in which each is at the orientation, location and scale that minimizes its distance from the reference while maintaining its key geometric proprieties in what is called the Kendall's shape space (Kendall, 1977; Small, 1996; Kendall et al., 2009). This is the essential algorithmic step preceding data analysis within the realm of GMM. After this algebraic procedure, most tools from multivariate statistics become applicable to any dataset of landmark multidimensional arrays (Zelditch et al., 2012; Benítez & Püschel, 2014).

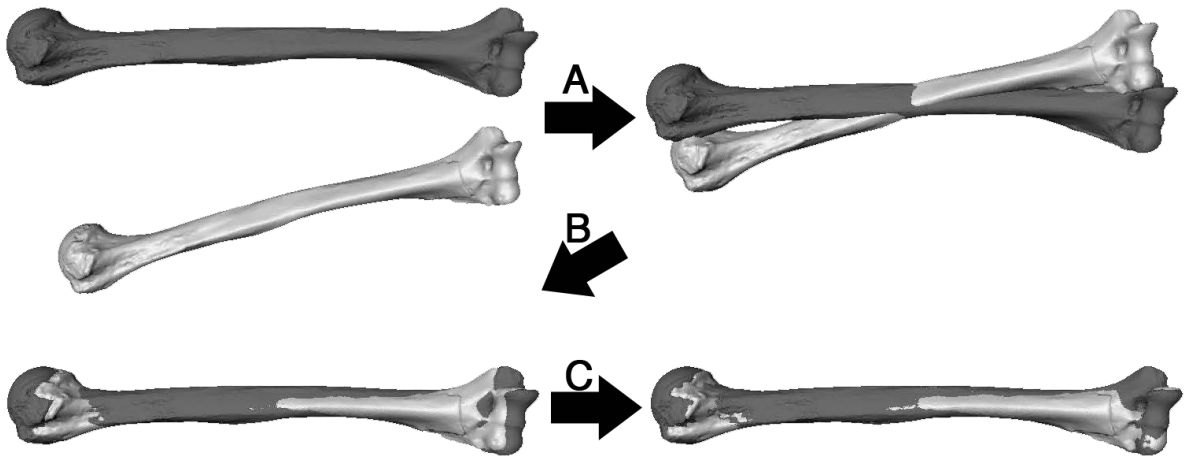

Figure 2-4 - Illustration of Procrustes Superimposition with the CEI/XXI 26 individual. Dark colored humerus represents the unburnt mesh and the lighter is the same bone after the heating experiment (900°C for 195 minutes). The GPA can be broken into 3 steps: A) translation, B) rotation and C) scaling. After A, B, C are performed, Procrustes Superimposition is achieved among the anatomical structures, meaning consensual shapes in Kendall's space were obtained and thus, these bones are ready for shape analysis.

There are two very important scalar vectors obtained from bringing our morphologies into the Kendall's shape space that seem to have practical correspondence to two critical concepts from burnt remains theory. The already mentioned Full Procrustes Distances (D_F) and differences in Centroid Size (CS) as independent quantitative measurements of heat-induced skeletal warping and shrinking, respectively. It should be noted that there are no references in the literature, previous to the publication of this manuscript, of a geometrically definable quantitative analysis of these two *phenomena*. Which together with fractures and color alterations represent the main spectrum of heat-induced skeletal changes (Gonçalves et al., 2014).

A simpler and older version of GPA is Ordinary Procrustes Analysis (OPA). Instead of performing a Procrustes superimposition for a whole sample, it is only applicable to 2 individuals. The mathematical steps for performing an OPA were actually laid down by renowned anthropologist Franz Boas (1905), for addressing shortcomings of using standard anatomical positioning (*e.g.* Frankfurt orientation). Later, it was reformulated for allowing matrix algebra calculations, to answer questions in psychometry (Mosier, 1939). Only with Gower (1975) does OPA gets generalized enough to allow infinite sample size, thus becoming known as GPA. Afterwards, much of the theoretical work that consolidated Procrustes superimposition as an elegant and mathematically coherent method of statistical shape theory is due to David Kendall (1984, 1985, 1989), who was initially motivated to apply superimposition algorithms in order to study shape and form characteristics of different megalithic sites (Broadbent, 1980; Kendall & Kendall, 1980).

For our purposes of addressing specific problems in burnt osteology, which includes estimating quantitatively warping and shrinking, we could either do OPA for every pair of unburt-and-burnt individual bone, or do a GPA for the whole sample. The second approach was preferred because it is far faster and easier to implement nowadays, and also because it gives us far more data. Since GPA is performed to the whole sample, it is possible to calculate all possible *Full Procrustes distances* among our 38 geometric individuals in the sample (i.e. a total of 384 Procrustes distances), even though only 19 of these are relevant to directly estimate warping. However, OPA is still a crucial concept for this thesis, in the sense that it is the only methodological way for others to test (with their own data) the predictive abilities of the statistical models that have been designed. Which are shown later in Chapter 3.7.

2.7 THIN-PLATE SPLINE INTERPOLATION

Grid plotting via interpolate functions had its roots in a simple, yet powerful idea of using deformation grids as a way for illustrating and formalize shape differences among geometrical entities. This intuition dates back to the 1528 manuscript by Albrecht Dürer on the variation of human proportions (Figure 2-5).

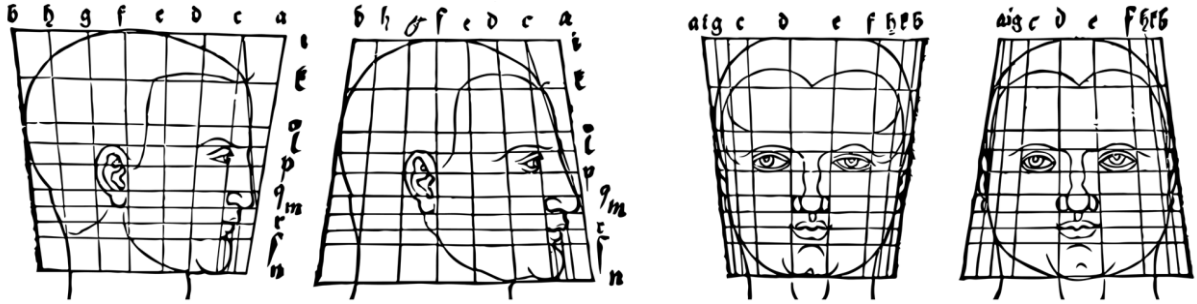

Figure 2-5 - A few examples of the first known use of deformation grids in anatomy. Vectorial graphics presented here were redrawn after Dürer's ([1528] 1969) original drawings.

Later in 1917, D'Arcy Thompson revisited the idea with what he called 'Cartesian transformations'. His insight was to not only use this tool for describing biological variability but also to apply it for interspecific form comparison (Figure 2-6). Yet Thompson ([1917] 1992) had also hand-drawn his grids, so these are actually also pre-Cartesian and error-prone. The one to solve this problem was Bookstein (1989), by implementing an interpolant function commonly used to address problems in material physics. With a TPS algorithm it is possible to computationally define a deformation grid from two sets of Cartesian coordinates. Thus effectively mapping the differences in form between two anatomical entities.

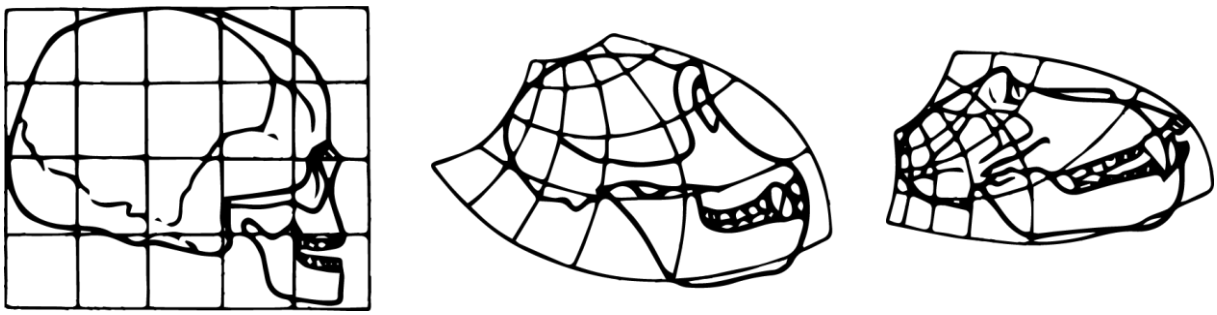

Figure 2-6 - Cartesian transformations from *Homo sapiens* into *Pan troglodytes* and a *Papio* sp. vectorial graphics adapted from Thompson's ([1917] 1992) classic *On Growth and Form*.

As a methodology TPS Interpolation serves 3 main goals in statistical shape analysis: (1) as it primary purpose it uses deformation grids as visualization tools of shape modification (Mitteroecker & Bookstein, 2011; Klingenberg, 2013); (2) it is used as well in dimensionality reduction, in the case of 3D data specifically from 3k degrees of freedom into 3k-7 with no loss of information. Obtaining the correct degrees of freedom allows the use of conventional statistical tests without having worries concerning complicated mathematical details (Zelditch et al., 2012); (3) additionally, it enables superimposition (sliding) of semilandmarks (Gunz & Mitteroecker, 2013).

For this thesis' objectives, the first point is perhaps the most crucial. But even if one was not concerned with graphical displays, TPS is useful since it performs an eigenanalysis of the bending energy matrix thus obtaining a parsimonious matrix that describes shape differences between a reference and another shape through partial warps scores, which can be directly used (unlike coordinates from GPA) for conventional statistical analysis, such as regression.

2.8 LOGISTIC MODEL TREES: A CLASSIFICATION ALGORITHM

The chosen Machine Learning algorithm to create our predictive models was Logistic Model Trees (LMT). It combines the heuristics of Logistic Regression and Decision Trees during its supervised training process. This is quite useful, since the former tends to show low variance, but high bias. While the later usually has low bias, but is less stable and prone to overfitting (Landwehr et al., 2005). In a recent preliminary study dealing also with a classification problem, LMT beat in overall accuracy many other state-of-the-art Machine Learning algorithms when trying to estimate sex from Procrustes-aligned shape matrices (Coelho et al., 2015).

For our dataset LMT is optimal, since the data we collected already has a bias and variance problem. Thus a classification algorithm that is robust to both problems is the most scientifically honest and sound approach. As a structured predictive model, it consists of a standard decision tree construction with logistic regression functions at its leaves (Figure 2-7). This makes it harder to interpret than simpler classification

algorithms, since it cannot be graphically represented as a tree of decisions neither as an elegant regression-style formula.

However, readers can still easily use any models created with LMT through loading their own landmark configurations into R and force an OPA between their obtained landmarks and our reference average shape, and then analyze their data by running the code provided in the following chapters.

```
LMT(examples){
   root <- new Node()
   alpha <- getCARTAlpha(examples)
   root.buildTree(examples, null)
   root.CARTprune(alpha)
}

buildTree(examples, inititalLinearModels){
   numIterations =
      CV_Iterations(examples, inititalLinearModels)
   initLogitBoost(initialLinearModels)
   linearModels <- copyOf(inititalLinearModels)
   for i = 1...numIterations{
      logitBoostIteration(linearModels, examples)
   }
   split <- findSplit(examples)
   localExamples <- split.splitExamples(examples)
   sons <- new Nodes[split.numSubsets()]
   for s = 1...sons.length{
      sons.buildTrees(localExamples[s], nodeModels)
   }
}


CV_Iterations(examples, initialModels) {
   for fold = 1...5 {
      initLogitBoost(inititalLinearModels)
      # split into training/test sets
      train <- trainCV(fold)
      test <- testCV(fold)
      linearModels <- copyOf(inititalLinearModels)
      for i = 1...200{
         logitBoostIteration(linearModels, train)
         logErros[i] += error(test)
      }
   }
   numIterations = findBestIteration(logErrrors)
   return numIterations
}
```

Figure 2-7 - Pseudocode for implementing Logistic Model Trees, (adapted from Landwehr et al., 2005)

3 RESULTS AND DISCUSSION

3.1 GETTING STARTED

All the results presented within this manuscript have been automatically generated as a .docx file through the `knitr` package for `R`. Even this paragraph itself was not written in Word, but instead in `R`. Contrary to the standard, this has the advantage of creating a text accompanied by the exact code that generated the graphics, tables and other results. Hence, increasing the reproducibility criteria, allowing other researchers to easily run the data analysis into their personal computers as long as they have data for it. This adheres to the tenants of the Open Data movement and Science 2.0 philosophy by promoting data analysis transparency among scientists.

If you desire to execute in your computer the whole data analysis present in this thesis you should first make sure to:

- Have installed `R` and the latest version of RStudio
- Install the latest version of the `knitr` package, by writing `install.packages("knitr")` in your RStudio console.

To run the code that produced my thesis output:

- Open RStudio, and go to File > New > R Markdown
- Paste in the contents of the `results.Rmd` available in this thesis' online repository http://git.io/vYjNa, or by contacting me: joao@osteomics.com
- Click **Knit Word**

You should not forget to use `setwd("YOUR/FOLDER/LOCATION")` to where the landmark files and 3D meshes are located. Or even easier, just open the **HOTProject-GM.Rproj** file, since it automatically loads everything.

It should run fine as long as you follow what is said above. Just to clarify, from here on, every time you see chunks of code, you can easily identify them through the box with light background and different font type that gets colored by association of the type of programming object. There you also see some commands that usually have a # symbol followed by some sentence, which are explanatory commentaries upon what the code is doing to help non-experts understanding what is being programmed. If it is a double ## it is an output generated by the code.

3.2 DATA INPUT

Our landmarks were obtained from the free software Landmark Editor. Likewise, it was attempted to use `auto3Dgm` for the same aim, and also in order to compare the two approaches (i.e. manual versus automatic). Nonetheless, as it can be seen in Figure 3-1 that was generated from the output of the `auto3Dgm` algorithm, a total of 5 burnt bones were inadequately aligned. Regrettably, this would effectively reduce the geometric *n* by 10, since their counterparts (i.e. the unburnt) would not be used for any particular purpose without their pair. Considering that no way was found within `R` to solve this problem, this approach was discontinued mid-way during the project because it would considerably reduce our *n*.

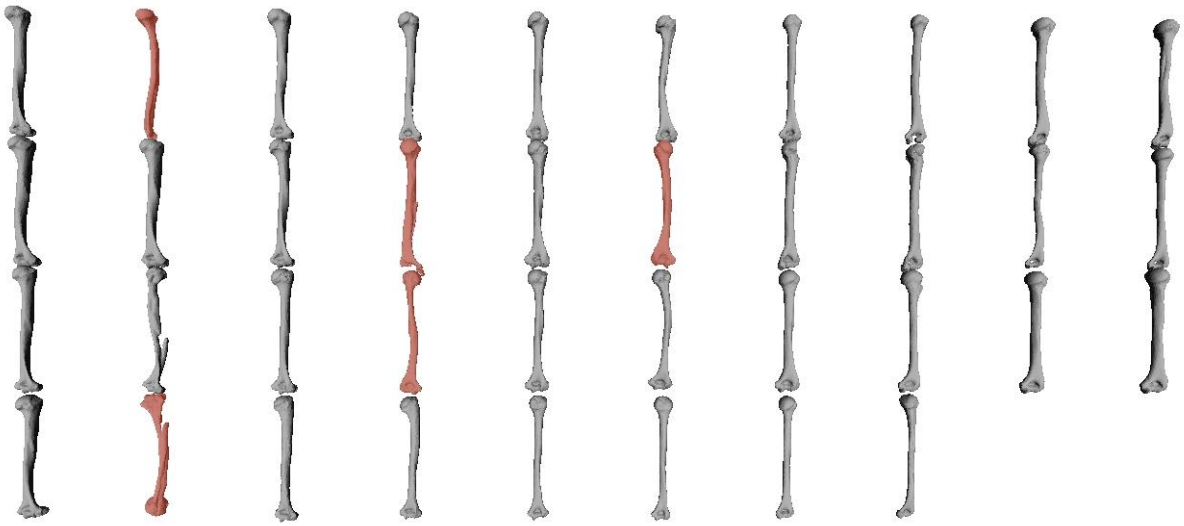

Figure 3-1 - Shapes automatically scaled and aligned by auto3Dgm using 256 pseudolandmarks. The incorrectly aligned bones are presented in red, which are all burnt *humeri* (of CEI/XXI 5, 32, 35, 51 and 65). Notice that some have been mirrored (turned into left antimeres), others were rotated 180 degrees in an axis and one was rotated in another axis and mirrored, overall very chaotic algebraic transformations. Despite hundreds of attempts, no elegant solution for this problem was found, and the use of auto3Dgm for this project was abandoned.

```
SW <- read.csv(file = './data/SingularWarps.csv', header = TRUE) # loads
all the variables that aren't shape-data.

rawdata <- pts2array(pts.dir = './data/pts-files') # loads raw landmark
data into R, similary to readland.nts(), check ?readland.nts

dimnames(rawdata)[[3]] # reads each geometric configuration's name. Useful
 to confirm if the order and naming are correct and consistent with
 singular warps order. Codenames have ID, sex and burning temperature.
```

```
##  [1] "CEIXXI05F"     "CEIXXI05F900"  "CEIXXI08F"     "CEIXXI08F700"
##  [5] "CEIXXI17M"     "CEIXXI17M900"  "CEIXXI24F"     "CEIXXI24F800"
##  [9] "CEIXXI26F"     "CEIXXI26F900"  "CEIXXI29M"     "CEIXXI29M800"
## [13] "CEIXXI32F"     "CEIXXI32F800"  "CEIXXI35M"     "CEIXXI35M900"
## [17] "CEIXXI43M"     "CEIXXI43M800"  "CEIXXI49F"     "CEIXXI49F850"
## [21] "CEIXXI50F"     "CEIXXI50F900"  "CEIXXI51M"     "CEIXXI51M900"
## [25] "CEIXXI53F"     "CEIXXI53F800"  "CEIXXI57M"     "CEIXXI57M900"
## [29] "CEIXXI64M"     "CEIXXI64M800"  "CEIXXI65F"     "CEIXXI65F900"
## [33] "CEIXXI79M"     "CEIXXI79M900"  "CEIXXI86M"     "CEIXXI86M1000"
## [37] "CEIXXI97F"     "CEIXXI97F1050"
```

3.3 DATA PRE-PROCESSING AND GPA

As result of poor preservation some *humeri* from our sample do not have anatomical parts where specific landmarks should be located. This was either due to taphonomic processes or because of the heating experiment itself. However, robust methods have been devised within statistical shape analysis in order to handle missing data. For solving this, the very convenient `estimate.missing()` function from the `geomorph` package is used to generate estimates of the missing landmarks.

```
EM <- estimate.missing(rawdata, method = 'TPS') # This command estimates
missing landmarks using either Thin Plate Spline or Regression. Here TPS
was chosen.
```

Preforming GPA over your data is the quintessential step to start a statistical shape analysis. In `geomorph` this is achieved with the `gpagen()` command. Our aligned Procrustes coordinates, and specimens' centroid sizes are recorded as the variables `procrustes$coords` and `procrustes$Csize`, respectively.

```
procrustes <- gpagen(EM, ShowPlot = FALSE) # Procrustes superimposition,
creates a viable dataset for applying geometric morphometrics methods.
```

Right now we have everything we need to start a multivariate statistical analysis of shape and its covariation with other variables (Bookstein, 1997a). However it is better to do some graphical exploration, in order to understand our data and correctly obtain fruitful inferences from it.

3.4 EXPLORATORY DATA ANALYSIS

An essential step of every data analysis that rarely takes the spotlight is the visual data exploration that antecedes inference or modeling. It is extremely important in the sense that allows us to allocate our precious time in more fruitful avenues, rather than trying everything for all the variables without a rigorous aim in mind.

The exploratory data analysis was broken into two main steps. First we intended to summarize, describe and visualize general aspects of our data. This was achieved in Table 1 and Figure 3-2, but also complemented with the Table 4 in Appendix 6.4. Second, we used a method based on the Geometric Morphometrics toolkit to look for possible errors in the landmark placing protocol.

3.4.1 DESCRIPTIVE STATISTICS

Now, we perform quick and very simple data manipulation to allow the construction of graphical plots and tables. We provide counts of values, and many classic measures developed by the theory of probability distributions.

```
logSize <- log(as.numeric(procrustes$Csize)) # The log of Centroid Size is
 useful and recommended in the literature for creating models.


Shapes <- procrustes$coords # Gives a new name easier to remember.

kable(stat.desc(cbind(logSize, SW[,-c(1:4)]), norm = TRUE), digits = 2) #
 Creates a table. Categorical variables were removed because most of these
 stats only make sense for numeric variables.
```

Table 1 - Descriptive statistics for the vectors of numeric variables in our dataset.

	logSize	months.buried	age	temperature	duration	mass
n of values	38.00	32.00	38.00	38.00	38.00	38.00
n of nulls	0.00	0.00	0.00	19.00	19.00	0.00
n of NA	0.00	6.00	0.00	0.00	0.00	0.00
min	6.35	71.00	70.00	0.00	0.00	23.20
max	6.69	84.00	90.00	1050.00	195.00	124.49
range	0.34	13.00	20.00	1050.00	195.00	101.29
sum	249.39	2358.00	3050.00	16500.00	2569.00	2588.03
median	6.59	73.00	81.00	350.00	37.50	62.16
mean	6.56	73.69	80.26	434.21	67.61	68.11
SE	0.01	0.52	1.02	71.96	11.64	4.44
CI95	0.03	1.06	2.08	145.80	23.59	9.00
variance	0.01	8.61	39.87	196770.98	5151.98	750.38
SD	0.09	2.93	6.31	443.59	71.78	27.39
var.coef	0.01	0.04	0.08	1.02	1.06	0.40
g1	-0.54	2.64	-0.11	0.05	0.26	0.33
SC-g1	-0.70	3.19	-0.14	0.06	0.34	0.43
g2	-0.65	6.63	-1.31	-1.99	-1.66	-1.01
SC-g2	-0.43	4.10	-0.88	-1.33	-1.11	-0.67
W	0.95	0.60	0.94	0.71	0.78	0.94
W's *p*-value	0.08	0.00	0.04	0.00	0.00	0.06

Legend: SE = Standard Error of the Mean; CI95 = Confidence Intervals of the Mean at 95%; SD = Standard Deviation; var.coef = variation coefficient; g1 = the skewness coefficient; SC-g1 = significant criterium of g1, if > 1 then skewness is significantly different than zero; g2 = kurtosis coefficient; SC-g2 = same definition as g1SC but for kurtosis; W = the statistic of a Shapiro-Wilk test of normality; W's *p*-value is the associated probability of the W statistic.

Next, we check potential correlations and possibility for regression models in our non-shape related data (i.e. Singular Warps) and the logarithm of Centroid Size. This last measure is also included because it is a vector of size and can be easily represented. Procrustes landmarks are a $p * k * x$ data matrix, in our case, a shape configuration of 35 landmarks, 3 dimensions and 38 individuals. Therefore, it would be too complicated to visualize through the graphical device of Figure 3-2 or Table 1 and so shape data was not included here.

```
scatterplotMatrix(cbind(logSize, SW[ ,-c(1,2)]), col = c('#f1c40f', '#e74c
3c', 'black'), lwd = 2)
```

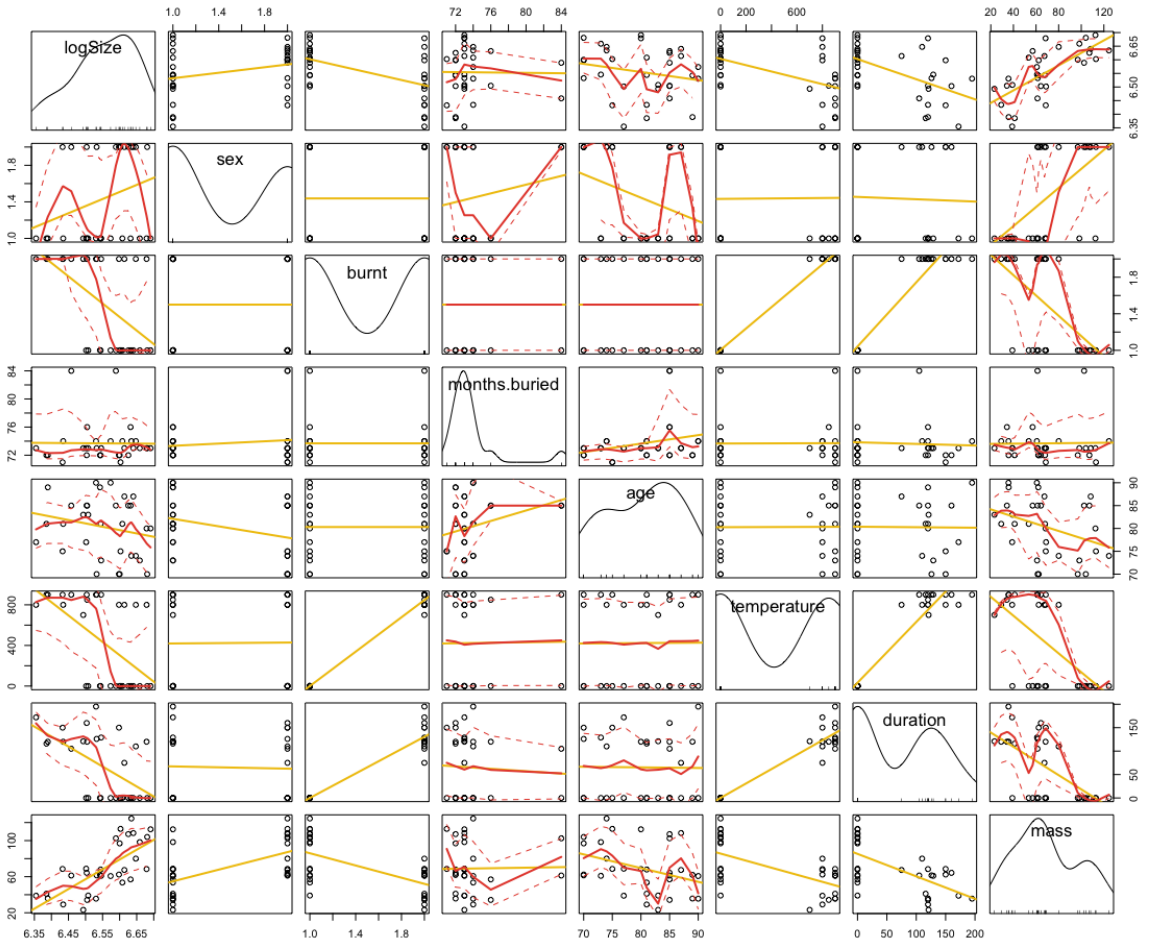

Figure 3-2 - Scatterplot matrix of our variables to visually complement the descriptive statistics of Table 1. Yellow lines are simple linear models (lm) while red lines are generalized additive models (GAM) with respective 95% confidence intervals in dashed red lines.

3.4.2 EXPLORATION OF UNCERTAINTY

Since we have seen how all the other variables are interacting, now we focus solely on our shape data. First, we try to see if there are any outliers in terms of landmark configurations within our dataset. This can be done with the `plotOutliers()` function, which is very useful because it allows researchers to verify if any specimen was incorrectly digitized (*e.g.* landmarks out of order or anatomically misplaced).

```
outliers <- plotOutliers(Shapes) # Plots potential outliers through
calculation of Procrustes Distance.
```

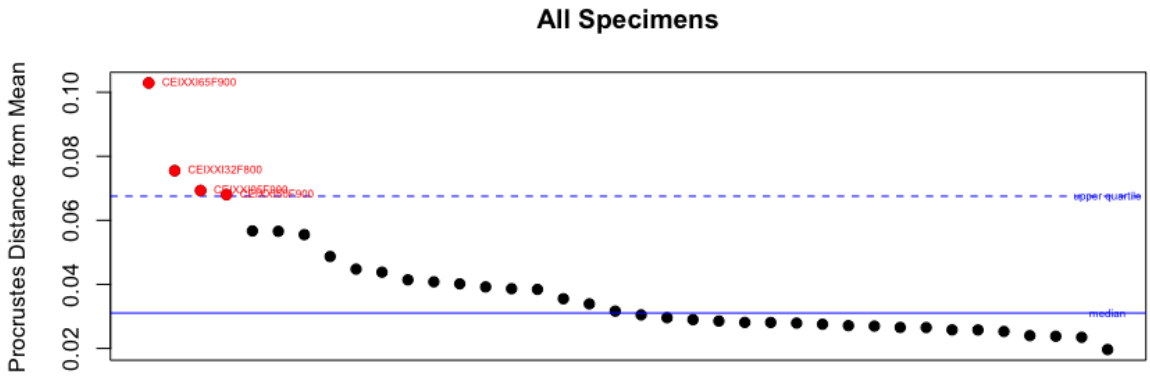

Figure 3-3 - Plot for potential shape outliers. After GPA, all 38 shapes in the sample were plotted, through Procrustes distances from Mean Shape. The burnt state of 4 different humeri deviate considerably from the average shape and so we could be looking at potentially outliers in our sample.

Interestingly, after a visual check in Landmark Editor, none of the "outliers" marked in red (Figure 3-3) had actually misplaced or disordered anatomical landmarks. These 4 appear as outliers because of how much heat-induced warping and fracturing affected their shape. Together, **CEI/XXI 65**, **32**, **5**, and **50** represent the most extremely modified-by-heat *humeri* within our sample. This can be confirmed visually with the 3D meshes files, but is also sustained by performing a PCA on our data.

3.5 PRINCIPAL COMPONENTS ANALYSIS

The following function plots a set of Procrustes-aligned specimens in tangent space along their principal axes (Figure 3-4). In our case the plot illustrated that all the bones before heating, and also the bones that were not much affected by the heating experiment tend to cluster around the *Origin* of the Cartesian plot of the two Principal Components. The more extremely modified by heat are dispersed in the periphery in what seems to be pseudorandom directions. A bigger dataset is needed to understand the patterns governing these directions, which are possibly describing different ways in which the bone is being deformed by heat.

```
# Define graphical proprieties of the PC plot:

gp <- as.factor(SW$temperature)
col.gp <- c('#bdc3c7', '#f1c40f', '#f39c12', '#e67e22', '#d35400', '#e74c3
c', '#c0392b') # Picking html colors for the plot
pch.gp <- c(12:18)
```

```
names(col.gp) <- levels(gp)
names(pch.gp) <- levels(gp)
col <- col.gp[match(gp, names(col.gp))]
pch <- pch.gp[match(gp, names(pch.gp))]

# Calculate a PCA:

y <- two.d.array(Shapes)
pc.res <- prcomp(y)
pcdata <- pc.res$x

# Code our plot:

plot(pcdata[, 1], pcdata[, 2], pch = pch, asp = 1, col = col, cex = 1.5, x
lab = paste('PC ', 1), ylab = paste('PC ', 2))
segments(min(pcdata[, 1]), 0, max(pcdata[, 1]), 0, lty = 2, lwd = 1)
segments(0, min(pcdata[, 2]), 0, max(pcdata[, 2]), lty = 2, lwd = 1)
text(pcdata[, 1], pcdata[, 2], dimnames(rawdata)[[3]], adj = c(-0.05, -0.7
), cex = 0.7)

# Add a legend:

legend(0.12, 0.04, legend = levels(gp), pch = pch.gp, col = col.gp)
```

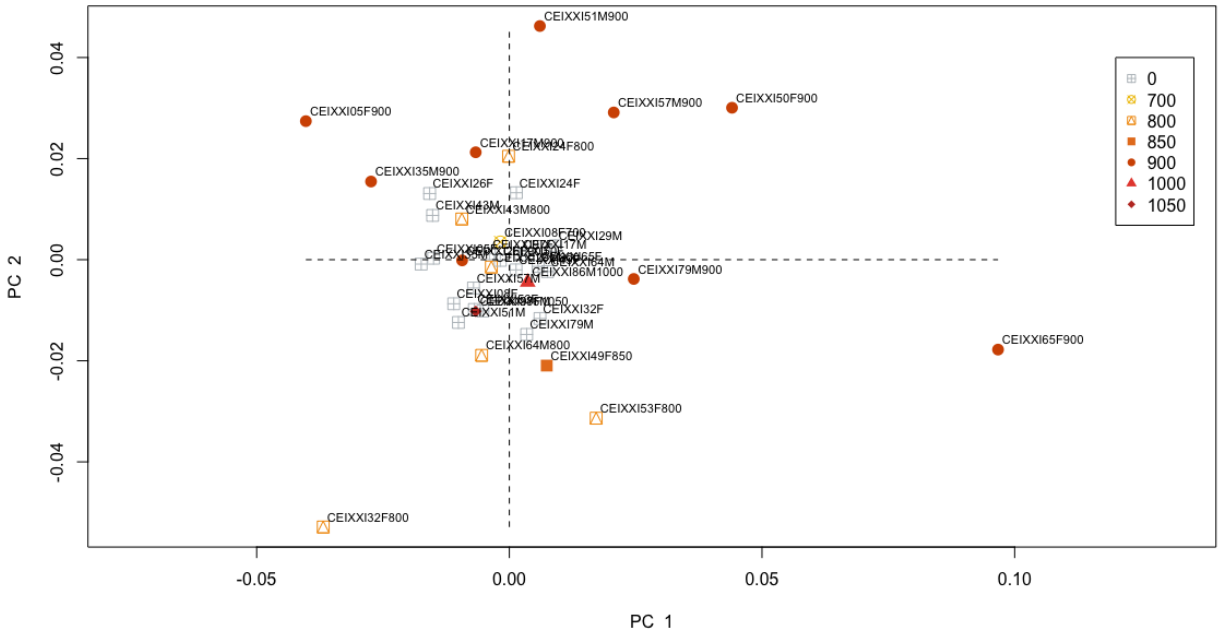

Figure 3-4 - Dataset projected onto PC1-2 Subspace. Together PC1+PC2 have a Cumulative Proportion of Variance = 0.4490, meaning they explain nearly half of the variance in our sample. The 0 value in temperature is actually a NULL value corresponding to the geometries of the unburnt counterparts.

One should never forget that ultimately, PCA is nothing more than a rotation of the original data. Its usefulness lies in the fact that our features will exhibit covariances

because they are influenced by and interact with common processes. The magnitudes of variances described by all components can be seen in Figure 3-5.

```
# To plot a graph of the proportion of variance explained by each PC:

pvar <- (pc.res$sdev^2)/(sum(pc.res$sdev^2))

names(pvar) <- seq(1:length(pvar))

barplot(pvar, main = 'Eigenvalues', xlab= 'Principal Components', ylab = '
% Variance', col = 'black', las = 2, cex.names = 1)
```

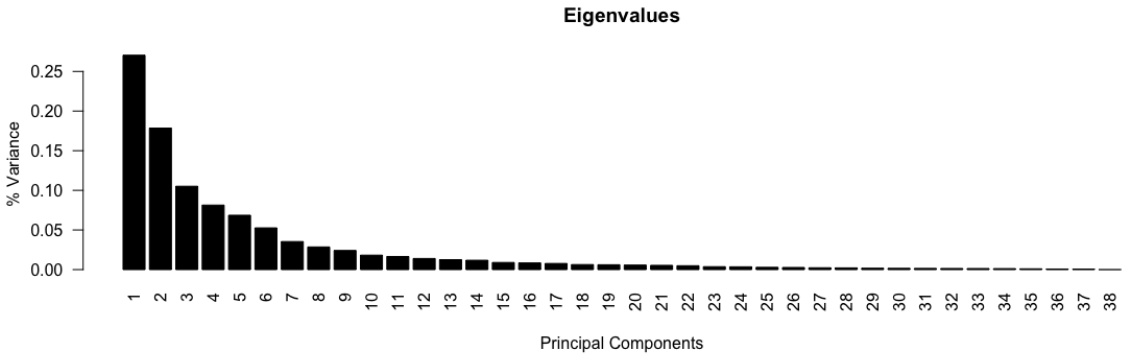

Figure 3-5 - Scree plot of the proportion of variance in descending order. The cumulative proportion of the first 13 PCs explain more than 90% of the variance in the shapes sample.

3.6 THIN-PLATE SPLINE PLOTS

Also important is to visualize the changes within a particular bone, between its pre-heating shape and deformed-by-heat shape through TPS (Figure 3-6). For achieving this, we generated thin-plate spline deformation grids. To visualize 3D data deformations into the paper format that bounds this thesis, thin-plate spline grids are show in the x-y and x-z axis (Figure 3-7). The y-z axis is not presented, because it is very difficult to understand anything from that perspective. Also, because the other two views in 2D are sufficient to show all the 3 axes from 3D already. Thus, a third view is redundant.

```
GP <- gridPar(pt.bg = 'black', pt.size = 0.5, n.col.cell = 25) # Defines
general graphical proprieties of the following plots.
```

```
plotRefToTarget(Shapes[,,1], Shapes[,,2], gridPars = GP, method = 'TPS') #
 TPS plot of CEIXXI05F
```

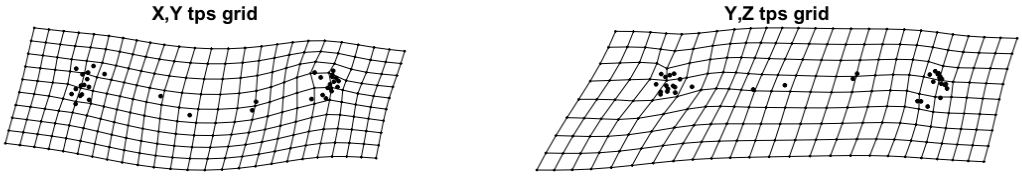

Figure 3-6 - TPS plot of individual CEI/XXI 5, with reference shape being the pre-heating state and deforming shape the post-heating shape. As it can be seen, even though there are only 4 landmarks in the diaphysis, these were enough to visually demonstrate the bending curvature resulting from the heat-induced skeletal warping which is most notable in the X-Y axes.

```
plotRefToTarget(Shapes[,,13], Shapes[,,14], gridPars = GP, method = 'TPS')
 # TPS plot of CEIXXI32F
```

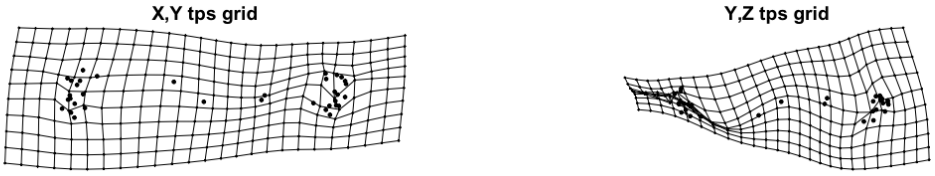

Figure 3-7 - TPS plot of individual CEI/XXI 32, with reference shape being the pre-heating state and deforming shape the post-heating shape. As it can be seen this bone has suffered considerable from the effects of heat-induced skeletal shrinking. Another interesting feature of individual 32 was that it fractured nearly the middle, what caused warping to create a rotational or torsion effect in the distal part of the humerus, this can be understood easily by looking at the left side of the Y-Z perspective.

Only individual CEI/XXI 5 and 32 are shown here in the results for illustrative purposes because having the whole dataset would take too much space. For more comprehensive results check the Appendix 6.6. There, a total of 19 TPS deformation plots can be found, fully describing the whole dataset.

3.7 PREDICTIVE MODELLING

"Essentially, all models are wrong, but some are useful."

— (George Box *in* Box & Draper, 1987: 424)

Creating models with such reduced sample sizes is usually not a good decision. Here, we create them, to show how easy it is to implement and test predictive models with our kind of data. While all models presented are already fully operational, it is hard to truly estimate their actual degree of accuracy. This is due to deficient implementation of cross-validation algorithms when dealing with badly represented factors and small *n*.

3.7.1 PROCRUSTES ANALYSES OF VARIANCE

A Procrustes ANOVA is used to quantify the relative amount of shape variation attributable to one or more variables in a linear model and assesses this variation through permutation. In `geomorph` the function `procD.lm()` allow us to input data by a y~X formula, where 'y' specifies the response variable (shape data), and 'X' contains one or more independent variables (Adams et al., 2015).

`procD.lm()` follows the philosophy that:

- Randomization procedures are used to generate empirical sampling distributions to assess significance of effects.
- Effect sizes are estimated as standard deviates from such sampling distributions.

The function performs statistical assessment of the terms in the model using Procrustes distances among specimens, instead of explained covariance matrices among variables. With this approach, the sum-of-squared Procrustes distances are used as a measure of SS and permutation is used to evaluate observed SS (Adams & Otárola-Castillo, 2013).

```
# The residual SS (RSS) of a linear model (also called the sum of squared
error, SSE) is found as follows:

RSS <- function(fit) sum(diag(resid(fit)%*%t(resid(fit))))

Sex <- SW$sex

fit1 <- lm(y ~ 1) # model contaning just an intercept
fit2 <- lm(y ~ logSize) # allometric scaling of shape
fit3 <- lm(y ~ logSize + Sex) # previous model + sexual dimorphism
fit4 <- lm(y ~ logSize * Sex) # previous model + interaction between sex
and log(CS)

# For any model 'fit', we can summarize the error of prediction by calcula
ting RSS.


RSS(fit1)

## [1] 0.06791796
```

```
RSS(fit2)
## [1] 0.06537494
RSS(fit3)
## [1] 0.06288619
RSS(fit4)
## [1] 0.05736431
kable(procD.lm(Shapes ~ logSize*Sex, RRPP = TRUE), digits = 4)
```

Table 2 - Procrustes ANOVA for shape data is being used as a tool for model comparison. A model where size takes sexual dismorphism into account is superior to the other, simpler models.

	df	SS	MS	Rsq	F	Z	P.value
logSize	1	0.0025	0.0025	0.0374	1.5073	1.3018	0.149
Sex	1	0.0025	0.0025	0.0366	1.4751	1.2981	0.144
logSize:Sex	1	0.0055	0.0055	0.0813	3.2728	2.9602	0.002
Residuals	34	0.0574	0.0017				
Total	37	0.0679					

In `procD.lm()` two resampling procedures are possible: (1) if `RRPP=FALSE`, the rows of the matrix of shape variables are resampled in relation to the design matrix; (2) if `RRPP=TRUE`, a residual randomization permutation procedure is utilized (Collyer et al., 2014). While similar for single-factor designs, when evaluating factorial models it has been shown that RRPP attains higher statistical power and thus is better at pattern-recognition (Anderson & Braak, 2003).

In the literature, the model we just created as been described as a Procrustes ANOVA (Goodall, 1991). However it is actually identical to the popular distance-based ANOVA designs (Anderson, 2001), except that it uses coordinates transformed through Procrustes superimposition. Our objective here is to show the ability of Procrustes ANOVA to compare models. As it is shown in Table 2 the model `fit4` that corresponds to size and sexual dimorphism interacting, outperforms the other simpler models. This same procedure could be repeated for many other variables and model designs, however having in consideration our unbalanced factors in most of the other relevant variables available it would be quite absurd to expect reliable error estimates (RSS) of most possible models. Also the R-Squared values obtained are currently too low to consider this models as useful for reliable predictions.

3.7.2 GROWING TREES INTO ANSWERS

The following model `lmtFit1` uses Logistic Model Trees (Landwehr et al., 2005) to predict if a humerus was burnt or not with 92.1% accuracy, by being trained on the first 8 Principal Components of our sample. So how should nonmorphometricians interested in burnt remains proceed to apply this model to a humerus from their own sample? By following the whole protocol: (1) 3D Scanning a humerus; (2) Processing it in MeshLab; (3) Obtain the defined 35 Landmarks for that bone; (4) Perform an OPA on the obtained configuration by using the mean shape of our sample as the reference shape; (5) perform a PCA on the configuration, (6) apply the model by using the `R` function `predict()` on his first 8 PCs. Alternatively, step 1, 2, and 3 could be substituted by obtaining landmarks directly from a MicroScribe or a similar device.

```
data.models <- cbind(SW[,-c(1, 2)], logSize, pcdata[ ,1:8])

lmtFit1 <- LMT(burnt ~ PC1+PC2+PC3+PC4+PC5+PC6+PC7+PC8, data = data.models
)
summary(lmtFit1)
```

```
##
## === Summary ===
##
## Correctly Classified Instances          35               92.1053 %
## Incorrectly Classified Instances         3                7.8947 %
## Kappa statistic                          0.8421
## Mean absolute error                      0.2245
## Root mean squared error                  0.297
## Relative absolute error                 44.8947 %
## Root relative squared error             59.4075 %
## Coverage of cases (0.95 level)         100      %
## Mean rel. region size (0.95 level)      97.3684 %
## Total Number of Instances               38
##
## === Confusion Matrix ===
##
##   a  b   <-- classified as burnt
##  18  1 |  a = no
##   2 17 |  b = yes
```

However, in most cases, for the trained osteologist it is easy to understand if a bone was burnt or not by just looking at it. Even if dealing with particularly complicated cases, there are already well established methods like Fourier Transform Infrared Spectroscopy (Munro et al., 2007; Thompson et al., 2009) or histological techniques that can erase most

doubts if they arise (Bradtmiller & Buikstra, 1984; Nelson, 1992; Hiller et al., 2003). So why would a model like this be useful? It would not: it is too time consuming. A far more useful model would be a similar one that could not only determine if a bone was burnt but at which maximum temperature it was burnt. Next, we implement such model in a similar fashion.

```
lmtFit2 <- LMT(as.factor(temperature) ~ PC1+PC2+PC3+PC4+PC5+PC6+PC7+PC8,
data = data.models)
summary(lmtFit2)

##
## === Summary ===
##
## Correctly Classified Instances          32               84.2105 %
## Incorrectly Classified Instances         6               15.7895 %
## Kappa statistic                          0.7415
## Mean absolute error                      0.1091
## Root mean squared error                  0.2116
## Relative absolute error                 54.8523 %
## Root relative squared error             68.3659 %
## Coverage of cases (0.95 level)         100      %
## Mean rel. region size (0.95 level)      56.391  %
## Total Number of Instances               38
##
## === Confusion Matrix ===
##
##   a  b  c  d  e  f  g   <-- classified as
##  19  0  0  0  0  0  0 |  a = 0
##   0  1  0  0  0  0  0 |  b = 700
##   4  0  2  0  0  0  0 |  c = 800
##   0  0  0  1  0  0  0 |  d = 850
##   1  0  0  0  8  0  0 |  e = 900
##   1  0  0  0  0  0  0 |  f = 1000
##   0  0  0  0  0  0  1 |  g = 1050
```

Despite the lack of values for each factor, plus the short range of maximum temperatures experimented with, which of course causes overfitting. Combined with the low diversity of the factors themselves, which forces us to use a classification algorithm for temperatures instead of a regression, our model `lmfit2` provided what seems to be very promising results (Overall Accuracy = 84.21%). Here is shown a stepping-stone from where one could eventually create a very powerful model by increase *n* in each of the factors of the dependent variable, in order to reduce overfitting while increasing or maintaining overall accuracy.

4 CONCLUSION

> "All anthropological analyses conducted on burned remains will be wholly and fundamentally inaccurate"
>
> — (Thompson, 2005: 6)

As a project aimed at improving the current methods in burnt remains theory, it is still in a long way from bringing any effective impact to the field. Sample size was a major problem that led most of the data analysis towards a theoretical *cul-de-sac*. Low sample size undermines reliability, reduces statistical power and reproducibility of results, while overestimating effect size (Stodden, 2015). It is therefore a problem that can only be overcome by keeping on collecting data, with a focus on well-balanced experimental design. Meaning that the factors within variables must not be so disproportionately represented as they actually are. For example: up to now, 9 skeletons were burnt at 900°C, other 6 at 800°C, and for all the other temperatures experimented with (500, 700, 850, 1000 and 1050°C) we have only one case representing each. Obviously this severely limits the predictive power of any model since you cannot train a machine-learning algorithm with only a few cases for each factor. Certainly there is no algorithm that will learn how to represent these in such conditions. In spite of that, many experimental studies in the burnt osteology literature have even smaller samples. There are the typical $n = 1$ studies (*e.g.* DeHaan & Nurbakhsh, 2001) that usually are about burning a carcass of an animal to record the effects. Others, such as Thurman and Willmore (1981) had burned 8 human *humeri* for their analysis; and Nugent (2010) attempted to estimate the biological profile of 19 cremated individuals, yet only 18 *humeri* were analyzed. Contrasting, our sample will keep on growing into the future, benefiting from being part of the HOT Project and the CEI/XXI. But again: the solution is to focus on good experimental design, just increasing *n* blindly will not be enough.

Unfortunately, my data analysis is also included in a project suffering from the 'myth of flesh', which shows an overall high prevalence in anthropological studies concerning taphonomy. It has been explained as a "(…) bias [that] manifests itself in experimental research and analyses that treat skeletal elements as though they had always existed without the encumbrances of skin, muscle, ligament and other soft tissues

(…)" (Haglund & Sorg, 1996: 3). Eventually, even if a reasonable sample size is reached in the future and powerful predictive models are created, one must first question: to what point would these be reliable when applied to burnt bones originating from forensic cases? Prudency is mandatory, since forceful generalization of specific models usually leads to worthless results. Current hypothesis state that soft tissues are not just restricting heat transfer differentially through their thickness and composition, but also cutting off the oxygen supply to the underlying bone (McKinley & Tech, 2015). This leads us to another problem: actual combustion *versus* just heat transfer.

Even though terms such as 'burning', 'burned' or 'burnt' have been used recurrently throughout this thesis, it is explicit that the experiment only deals with thermally modified bones, which were not actually burned amid fire. Consequently, other variables that are not being accounted for, that can also bias any predictions to real-life situations, are the type and quantity of fuel, plus oxygen content or supply. Such variables are of the uttermost importance when dealing with combustion (i.e. fire), but do not really interfere with heat-transfer in the absence of combustion. Thus, it would be senseless for us to account for these, even though such variables are possibly very pertinent in arsons, mass disasters, various ethno-historic or archaeological types of cremation, and so on (DeHaan, 2015).

Until now, the reader might believe that no remarkable positive conclusions can be achieved in this particular line of research. But by using a metaphor that would work much better if a particularly famous movie title was written backwards: we just passed through the Ugly and the Bad. So, now comes the Good.

Is thermally modified dry bone that different from typical human burnt remains? Throughout the years evidences have come up, suggesting the gap between both might be far shorter than previously thought. Until demonstrated otherwise (Buikstra & Swegle, 1989; Spennemann & Colley, 1989), most literature attributed warping as a *phenomenon* exclusive of hydrated bones. Many papers (Baby, 1954; Binford, 1963; Thurman & Willmore, 1981; Etxéberria, 1994) interpreted presence of warping as a discriminant factor between burnings with prior tissue removal as opposed to excarnation absence. Meaning that at least 35 years of burnt osteology up to that point, worked on unsupported and false assumptions on one of its most basic aspects. Heating experiments under controlled conditions are thus crucial for busting myths, creating insights, and stimulating progress within this scientific domain (Thompson, 2005, 2009). But as have been

continuously cautioned, there are many problems that should be rigorously addressed. If so, this kind of research might bring tremendously value for forensic anthropologist and others dealing with human burnt remains.

It was demonstrated how to craft predictive models for estimating burning conditions such as maximum temperature and it was discussed how to improve the ones that have been created in the context of this thesis. If this research continues, these models will hopefully become powerful enough to be used by other researchers without any major obstacles. Even if such is not bound to happen with this particular research, it might inspire other colleagues to obtain their own data and create their own models based on the toolkit of GMM and ML algorithms. Since this was demonstrated here to be a possible route, which still needs to be much more explored for the thermally modified bones problematic.

Finally, it cannot be stressed enough how digital 3D preservation of anatomical structures exposed to heat is essential and how staggering it is that it as been pretty much dismissed, with the only exception found in literature being Imaizumi et al. (2014). Subjecting osteological material to heat is a great source of data with potential to infer not just correlation, but also causation. Simultaneously, without the proper protocol a considerable amount of data gets destroyed as well during the process. Collecting measurements such as lengths, mass and so on can be useful, but it is far from enough. Perhaps most of the field is unaware of the analytical possibilities brought by having data preserved in virtual 3D files. Even Imaizumi et al. (2014) used their collected CT scans solely for the purpose of calculating volumetric differences. Which is possibly one of the best ways to directly measure shrinkage, but offers no possibilities for warping quantification. Awareness of GMM and the possibility of curating 3D databases must be brought into burnt osteology, or otherwise knowledge that is clearly within grasp will continue to escape us.

Models should be created with other bones as well, besides the humerus. Actually, it was originally intended to use both *femura* and *humeri*, alas it was impossible. Because after the experiment, femurs almost always collapsed on their own weight, having fragmentation and far more extreme fractures, thus being overall more fragile (Figure 4-1). Following, the final *n* of femurs that could be 3D scanned before and after heating was so small that would be insane to try to perform any analysis with the few obtained 3D meshes. However tibiae and ulnae tend to preserve well and can be 3D scanned in an

identical protocol to the one provided earlier. Foot bones also tend to preserve considerably well, regrettably these do not tend to show alterations with such exuberance. For future attempts it is recommend that other researchers virtually preserve the tridimensional meshes of as many bones that will be subjected to experimental heating as possible, since these have high potential for improving current models and creating new ones. The methods devised here are yet to be explored and performed into any other burnt bones.

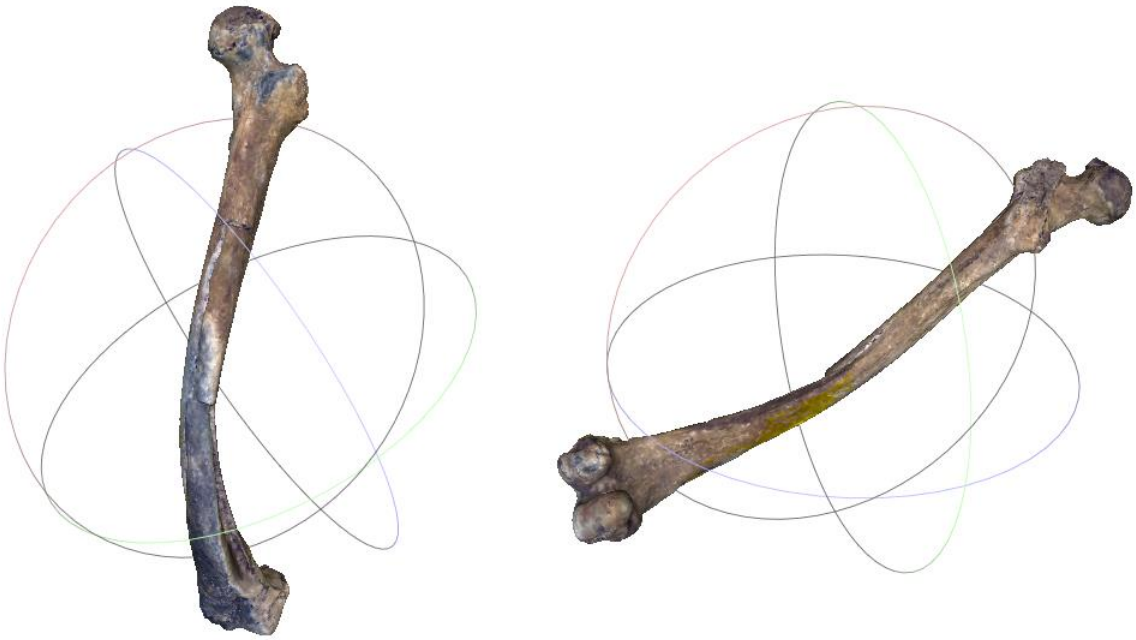

Figure 4-1 - Left femur of individual CEI/XXI 32 after being burnt at 800°C for 120 minutes, from two different perspectives. Even though the bone was flawlessly 3D scanned and digitally curated for posterity, it was broken in half during the process, which demonstrates its inherent fragility. Yet, the fact that a complete 3D model could be attained from a fragmented bone shows some promise for digital forensic reconstruction of fragmented burnt bones. This is yet another point in favor of using 3D laser scanning technologies that should be further explored in the future.

Ultimately, Thompson's quote in the beginning of the Conclusion is still as pertinent as it was 10 years ago. Nevertheless, with rigorous implementation of different methodologies, perhaps anthropological analyses conducted on burned remains do not need to keep on being "wholly and fundamentally inaccurate" and rather being only partially inaccurate, under some controlled error. Which is a far less lurid perspective; as I just passed by to bring you hope.

5 BIBLIOGRAPHY

Adams, D. C.; Otárola-Castillo, E. 2013. geomorph: an r package for the collection and analysis of geometric morphometric shape data. *Methods in Ecology and Evolution*. 4(4):393–399. DOI: 10.1111/2041-210X.12035.

Adams, D.; Collyer, M.; Sherratt, E. 2015. *geomorph: Geometric Morphometric Analyses of 2D/3D Landmark Data*. Available: http://cran.r-project.org/web/packages/geomorph/index.html [2015, June 14].

Adams, D. C.; Rohlf, F. J.; Slice, D. E. 2013. A field comes of age: geometric morphometrics in the 21st century. *Hystrix, the Italian Journal of Mammalogy*. (1). DOI: 10.4404/hystrix-24.1-6283.

Anderson, M. J. 2001. A new method for non-parametric multivariate analysis of variance. *Austral Ecology*. 26(1):32–46. DOI: 10.1111/j.1442-9993.2001.01070.pp.x.

Anderson, M.; Braak, C. ter. 2003. Permutation tests for multi-factorial analysis of variance. *Journal of Statistical Computation and Simulation*. 73(2):85–113. DOI: 10.1080/00949650215733.

Baby, R. S. 1954. Hopewell Cremation Practices. *The Ohio Historical Society Papers in Archaeology*. 1:1–7.

Benítez, H. A.; Püschel, T. A. 2014. Modelando la Varianza de la Forma: Morfometría Geométrica Aplicaciones en Biología Evolutiva. *International Journal of Morphology*. 32(3):998–1008. DOI: 10.4067/S0717-95022014000300041.

Binford, L. R. 1963. An Analysis of Cremations from Three Michigan Sites. *Wisconsin Archeologist*. 44:98–110.

Boas, F. 1905. The Horizontal Plane of the Skull and the General Problem of the Comparison of Variable Forms. *Science*. 21(544):862–863.

Bolitho, M.; Kazhdan, M.; Burns, R.; Hoppe, H. 2009. Parallel Poisson Surface Reconstruction. In *Advances in Visual Computing (Lecture Notes in Computer Science no. 5875)*. G. Bebis, R. Boyle, B. Parvin, D. Koracin, Y. Kuno, J. Wang, J.-X. Wang, J. Wang, R. Pajarola, P. Lindstrom, A. Hinkenjann, M.L. Encarnação, C.T. Silva, & D. Coming, Eds. Springer Berlin Heidelberg. 678–689.

Bonhomme, V.; Picq, S.; Gaucherel, C.; Claude, J. 2014. Momocs: Outline Analysis Using R. *Journal of Statistical Software*. 56(13):1–24.

Bookstein, F. L. 1989. Principal warps: Thin-plate splines and the decomposition of deformations. *IEEE Transactions on Pattern Analysis & Machine Intelligence*. (6):567–585.

Bookstein, F. L. 1997a. *Morphometric tools for landmark data: geometry and biology*. Cambridge University Press.

Bookstein, F. L. 1997b. Landmark methods for forms without landmarks: morphometrics of group differences in outline shape. *Medical Image Analysis*. 1(3):225–243. DOI: 10.1016/S1361-8415(97)85012-8.

Bookstein, F. L.; Gunz, P.; Mitteröcker, P.; Prossinger, H.; Schaefer, K.; Seidler, H. 2003. Cranial integration in Homo: singular warps analysis of the midsagittal plane in ontogeny and evolution. *Journal of Human Evolution*. 44(2):167–187.

Box, G. E. P. 1966. Use and abuse of regression. *Technometrics*. 8(4):625–629.

Box, G. E. P.; Draper, N. R. 1987. *Empirical Model-Building and Response Surfaces*. 1st ed. New York, Wiley.

Boyer, D. M.; Puente, J.; Gladman, J. T.; Glynn, C.; Mukherjee, S.; Yapuncich, G. S.; Daubechies, I. 2015. A New Fully Automated Approach for Aligning and Comparing Shapes. *The Anatomical Record*. 298(1):249–276. DOI: 10.1002/ar.23084.

Bradtmiller, B.; Buikstra, J. E. 1984. Effects of burning on human bone microstructure: a preliminary study. *Journal of Forensic Sciences*. 29(2):535–540.

Broadbent, S. 1980. Simulating the Ley Hunter. *Journal of the Royal Statistical Society. Series A (General)*. 143(2):109–140. DOI: 10.2307/2981985.

Bruzek, J.; Murail, P. 2006. Methodology and Reliability of Sex Determination From the Skeleton. In *Forensic Anthropology and Medicine*. A. Schmitt, E. Cunha, & J. Pinheiro, Eds. Humana Press. 225–242.

Buikstra, J. E.; Swegle, M. 1989. Bone modification due to burning: experimental evidence. In *Bone modification*. R. Bonnichsen & M.H. Sorg, Eds. Orono, ME, Center for the Study of the First Americans, Institute of Quaternary Studies, University of Maine. 247–258.

Campbell, N. A.; Atchley, W. R. 1981. The Geometry of Canonical Variate Analysis. *Systematic Zoology*. 30(3):268–280. DOI: 10.2307/2413249.

Chang, W. 2012. *R Graphics Cookbook*. Sebastopol, USA, O'Reilly Media.

Chinnery, B. 2004. Morphometric Analysis of Evolutionary Trends in the Ceratopsian Postcranial Skeleton. *Journal of Vertebrate Paleontology*. 24(3):591–609.

Cignoni, P.; Callieri, M.; Corsini, M.; Dellepiane, M.; Ganovelli, F.; Ranzuglia, G. 2008. MeshLab: an Open-Source Mesh Processing Tool. *Eurographics Italian Chapter Conference*. 129–136.

Claes, P.; Reijniers, J.; Shriver, M. D.; Snyders, J.; Suetens, P.; Nielandt, J.; De Tré, G.; Vandermeulen, D. 2015. An investigation of matching symmetry in the human pinnae with possible implications for 3D ear recognition and sound localization. *Journal of Anatomy*. 226(1):60–72. DOI: 10.1111/joa.12252.

Claude, J. 2008. *Morphometrics with R*. Springer Science & Business Media.

Coelho, J.; Navega, D.; Cunha, E. 2015. Sex Diagnosis Through Automated 3D Geometric Morphometrics of the Tali Bones. In *Conference: II Bioanthropological Meeting*. Coimbra, Portugal.

Collyer, M. L.; Sekora, D. J.; Adams, D. C. 2014. A method for analysis of phenotypic change for phenotypes described by high-dimensional data. *Heredity*. DOI: 10.1038/hdy.2014.75.

Cunha, E.; Baccino, E.; Martrille, L.; Ramsthaler, F.; Prieto, J.; Schuliar, Y.; Lynnerup, N.; Cattaneo, C. 2009. The problem of aging human remains and living individuals: a review. *Forensic Science International*. 193(1-3):1–13. DOI: 10.1016/j.forsciint.2009.09.008.

Curate, J. F. T. 2011. *O perímetro do declínio: osteoporose e fracturas de fragilidade em três amostras osteológicas identificadas portuguesas - séculos XIX e XX*. Tese de doutoramento em Antropologia Biológica. Faculdade de Ciências e Tecnologia da Universidade de Coimbra.

DeHaan, J. D. 2015. 1 - Fire and Bodies. In *The Analysis of Burned Human Remains*. C.W. Schmidt & S.A. Symes, Eds. San Diego, Academic Press. 1–13.

DeHaan, J. D.; Nurbakhsh, S. 2001. Sustained combustion of an animal carcass and its implications for the consumption of human bodies in fires. *Journal of Forensic Sciences*. 46(5):1076–1081.

Dirkmaat, D. C.; Cabo, L. L.; Ousley, S. D.; Symes, S. A. 2008. New perspectives in forensic anthropology. *American Journal of Physical Anthropology*. Suppl 47:33–52. DOI: 10.1002/ajpa.20948.

Dryden, I. L. 2014. *shapes: Statistical shape analysis*. Available: http://CRAN.R-project.org/package=shapes [2015, June 15].

Dryden, I. L.; Mardia, K. V. 1998. *Statistical Shape Analysis*. New York, Wiley.

Dürer, A. [1528] 1969. *Vier Bücher von Menschlicher Proportionen*. facsimile ed. Zürich, J. Stocker-Schmid. (Original work published in 1528).

Estellers, V.; Scott, M.; Tew, K.; Soatto, S. 2015. Robust Poisson Surface Reconstruction. In *Scale Space and Variational Methods in Computer Vision (Lecture Notes in Computer*

Science no. 9087). J.-F. Aujol, M. Nikolova, & N. Papadakis, Eds. Berlin, Springer International Publishing. 525–537.

Etxéberria, F. 1994. Aspectos macroscópicos del hueso sometido al fuego. Revisión de las cremaciones descritas en el País Vasco desde la Arqueología. *Munibe Antropologia-Arkeologia*. (46):111–116.

Fairgrieve, S. I. 2007. *Forensic Cremation Recovery and Analysis*. 1st ed. Boca Raton, CRC Press.

Ferreira, M. T.; Vicente, R.; Navega, D.; Gonçalves, D.; Curate, F.; Cunha, E. 2014. A new forensic collection housed at the University of Coimbra, Portugal: The 21st century identified skeletal collection. *Forensic Science International*. 245C:202.e1–202.e5. DOI: 10.1016/j.forsciint.2014.09.021.

Filiault, M. T. 2012. *Digitization Protocols and Applications for Laser Scanning Human Bone in Forensic Anthropology*. Honors in the Major Program in Anthropology. University of Central Florida.

Gandrud, C. 2013. *Reproducible Research with R and R Studio*. Boca Raton, Chapman and Hall/CRC.

Gonçalves, D. 2012. The micro-analysis of human burned bones: some remarks. *Cadernos do GEEvH*. 1(1):32–40.

Gonçalves, D.; Thompson, T. J. U.; Cunha, E. 2011. Implications of heat-induced changes in bone on the interpretation of funerary behaviour and practice. *Journal of Archaeological Science*. 38(6):1308–1313. DOI: 10.1016/j.jas.2011.01.006.

Gonçalves, D.; Thompson, T. J. U.; Cunha, E. 2013. Osteometric sex determination of burned human skeletal remains. *Journal of Forensic and Legal Medicine*. 20(7):906–911. DOI: 10.1016/j.jflm.2013.07.003.

Gonçalves, D.; Cunha, E.; Thompson, T. J. U. 2014. Estimation of the pre-burning condition of human remains in forensic contexts. *International Journal of Legal Medicine*. (May, 31):1–7. DOI: 10.1007/s00414-014-1027-8.

Gonçalves, D.; Coelho, J.; Gouveia, M.; Makhoul, C.; Santos, I.; Vassalo, A.; Santos, A. L.; de Carvalho, L. B.; Cunha, E. 2015. The Hot topic of burned human skeletal remains: Coimbra's contribution to Forensic Anthropology. In *Conference: International Symposium on Anthropology and Natural Disasters*. Coimbra, Portugal.

Goodall, C. 1991. Procrustes methods in the statistical analysis of shape. *Journal of the Royal Statistical Society. Series B (Methodological)*. 285–339.

Gower, J. C. 1975. Generalized procrustes analysis. *Psychometrika*. 40(1):33–51. DOI: 10.1007/BF02291478.

Green, W. D. K. 1996. The thin-plate spline and images with curving features. In *Image Fusion and Shape Variability Techniques: Proceedings*. K.V. Mardia, C.A. Gill, & I.L. Dryden, Eds. Leeds, Leeds University Press. 79–87.

Grupe, G.; Hummel, S. 1991. Trace element studies on experimentally cremated bone. I. Alteration of the chemical composition at high temperatures. *Journal of Archaeological Science*. 18(2):177–186. DOI: 10.1016/0305-4403(91)90046-R.

Gunz, P.; Mitteroecker, P. 2013. Semilandmarks: A Method for Quantifying Curves and Surfaces. *Hystrix, the Italian Journal of Mammalogy*. (1). DOI: 10.4404/hystrix-24.1-6292.

Haglund, W. D.; Sorg, M. H. 1996. Introduction to Forensic Taphonomy. In *Forensic Taphonomy*. Boca Raton, FL, CRC Press. 1–9.

Hiller, J. C.; Thompson, T. J. U.; Evison, M. P.; Chamberlain, A. T.; Wess, T. J. 2003. Bone mineral change during experimental heating: an X-ray scattering investigation. *Biomaterials*. 24(28):5091–5097.

Holden, J. L.; Phakey, P. P.; Clement, J. G. 1995a. Scanning electron microscope observations of incinerated human femoral bone: a case study. *Forensic Science International*. 74(1-2):17–28.

Holden, J. L.; Phakey, P. P.; Clement, J. G. 1995b. Scanning electron microscope observations of heat-treated human bone. *Forensic Science International*. 74(1–2):29–45. DOI: 10.1016/0379-0738(95)01735-2.

Holliday, T. W.; Friedl, L. 2013. Hominoid humeral morphology: 3D morphometric analysis. *American Journal of Physical Anthropology*. 152(4):506–515. DOI: 10.1002/ajpa.22385.

Horton, N. J.; Kleinman, K. 2015. *Using R and RStudio for Data Management, Statistical Analysis, and Graphics*. 2nd ed. Boca Raton, FL, Chapman and Hall/CRC.

Huxley, A. K.; Kósa, F. 1999. Calculation of percent shrinkage in human fetal diaphyseal lengths from fresh bone to carbonized and calcined bone using Petersohn and Köhler's data. *Journal of Forensic Sciences*. 44(3):577–583.

Imaizumi, K.; Taniguchi, K.; Ogawa, Y. 2014. DNA survival and physical and histological properties of heat-induced alterations in burnt bones. *International Journal of Legal Medicine*. 128(3):439–446. DOI: 10.1007/s00414-014-0988-y.

Kazhdan, M.; Hoppe, H. 2013. Screened poisson surface reconstruction. *ACM Transactions on Graphics (TOG)*. 32(3):29.

Kazhdan, M.; Bolitho, M.; Hoppe, H. 2006. Poisson surface reconstruction. In *Proceedings of the fourth Eurographics symposium on Geometry processing*. V. 7 Cagliari, Sardinia, Italy.

Kendall, D. G. 1977. The Diffusion of Shape. *Advances in Applied Probability*. 9(3):428–430. DOI: 10.2307/1426091.

Kendall, D. G. 1984. Shape Manifolds, Procrustean Metrics, and Complex Projective Spaces. *Bulletin of the London Mathematical Society*. 16(2):81–121. DOI: 10.1112/blms/16.2.81.

Kendall, D. G. 1985. Exact Distributions for Shapes of Random Triangles in Convex Sets. *Advances in Applied Probability*. 17(2):308–329. DOI: 10.2307/1427143.

Kendall, D. G. 1989. A Survey of the Statistical Theory of Shape. *Statistical Science*. 4(2):87–99. DOI: 10.1214/ss/1177012582.

Kendall, D. G.; Kendall, W. S. 1980. Alignments in Two-Dimensional Random Sets of Points. *Advances in Applied Probability*. 12(2):380–424. DOI: 10.2307/1426603.

Kendall, D. G.; Barden, D.; Carne, T. K.; Le, H. 2009. *Shape and Shape Theory*. John Wiley & Sons.

Klingenberg, C. P. 2013. Visualizations in geometric morphometrics: how to read and how to make graphs showing shape changes. *Hystrix - Italian Journal of Mammalogy*. 24(1):15–24. DOI: http://dx.doi.org/10.4404/hystrix-24.1-7691.

Kranioti, E. F.; Bastir, M.; Sánchez-Meseguer, A.; Rosas, A. 2009. A geometric-morphometric study of the Cretan humerus for sex identification. *Forensic Science International*. 189(1-3):111.e1–8. DOI: 10.1016/j.forsciint.2009.04.013.

Landwehr, N.; Hall, M.; Frank, E. 2005. Logistic Model Trees. *Machine Learning*. 59(1-2):161–205. DOI: 10.1007/s10994-005-0466-3.

Makhoul, C.; Coelho, J.; Gouveia, M.; Santos, I.; Vassalo, A.; Ferreira, M. T.; Cunha, E.; Gonçalves, D. 2015. The Protocol for the Preparation of Burned Identified Skeletons of the CEI/XXI Collection. In *Conference: II Bioanthropological Meeting*. Coimbra, Portugal.

Mayne-Correia, P. M. 1997. Fire Modification of Bone: a review of the literature. In *Forensic taphonomy: The postmortem fate of human remains*. W.D. Haglund & M.H. Sorg, Eds. New York, CRC Press. 275–294.

McKinley, J. L. 2000. The analysis of cremated bone. In *Human Osteology: In Archaeology and Forensic Science*. A. Cox & S. Mays, Eds. London, United Kingdom, Greenwhich Medical Media Ltd. 403–421.

McKinley, J. I.; Tech, B. 2015. 10 - In the Heat of The Pyre. In *The Analysis of Burned Human Remains*. C.W. Schmidt & S.A. Symes, Eds. San Diego, Academic Press. 163–xiv.

Mitteroecker, P.; Bookstein, F. 2011. Linear Discrimination, Ordination, and the Visualization of Selection Gradients in Modern Morphometrics. *Evolutionary Biology*. 38(1):100–114. DOI: 10.1007/s11692-011-9109-8.

Mitteroecker, P.; Gunz, P. 2009. Advances in Geometric Morphometrics. *Evolutionary Biology*. 36(2):235–247. DOI: 10.1007/s11692-009-9055-x.

Mosier, C. I. 1939. Determining a simple structure when loadings for certain tests are known. *Psychometrika*. 4(2):149–162. DOI: 10.1007/BF02288493.

Munro, L. E.; Longstaffe, F. J.; White, C. D. 2007. Burning and boiling of modern deer bone: Effects on crystallinity and oxygen isotope composition of bioapatite phosphate. *Palaeogeography, Palaeoclimatology, Palaeoecology*. 249(1-2):90–102. DOI: 10.1016/j.palaeo.2007.01.011.

Navega, D.; Coelho, C.; Vicente, R.; Ferreira, M. T.; Wasterlain, S.; Cunha, E. 2014. AncesTrees: ancestry estimation with randomized decision trees. *International Journal of Legal Medicine*. (July, 23). DOI: 10.1007/s00414-014-1050-9.

Nelson, R. 1992. A microscopic comparison of fresh and burned bone. *Journal of Forensic Sciences*. 37(4):1055–1060.

NextEngine™, I. 2015. *HD Desktop 3D scanner and ScanStudio™*. Santa Monica, California., NextEngine™, Incorporated. Available: http://nextengine.com.

Nietzsche, F. [1878–1880] 1996. *Human, All Too Human: A Book for Free Spirits*. 2nd ed. New York, Cambridge University Press. (Original work published in 1878–1880).

Nugent, T. G. 2010. *The Estimation of Biological Profile From Unprocessed Human Cremated Remains*. artial Fulfillment of the Requirements for the Degree of Master of Arts. Texas State University.

Payne-James, J.; Busuttil, A.; Smock, W. 2003. *Forensic Medicine: Clinical and Pathological Aspects*. Cambridge University Press.

Popper, S. K. R. 1959. *The logic of scientific discovery*. London, United Kingdom, Hutchinson.

Randolph-Quinney, P. 2014a. Burnt Human Remains Part 2 - Identification and Laboratory Analysis. In *Advances in Forensic Human Identification*. X. Mallet, T. Blythe, & R. Berry, Eds. New York, CRC Press. 145–164.

Randolph-Quinney, P. 2014b. Burnt Human Remains Part 1 - Fire Dynamics and Body Recovery. In *Advances in Forensic Human Identification*. X. Mallet, T. Blythe, & R. Berry, Eds. New York, CRC Press. 127–144.

R Core Team. 2015. *R: A Language and Environment for Statistical Computing*. Vienna, Austria, R Foundation for Statistical Computing. Available: http://R-project.org/.

Rogers, R. G.; Everett, B. G.; Saint Onge, J. M.; Krueger, P. M. 2010. Social, Behavioral, and Biological Factors, and Sex Differences in Mortality. *Demography*. 47(3):555–578.

Rohlf, F. J.; Corti, M. 2000. Use of two-block partial least-squares to study covariation in shape. *Systematic Biology*. 49(4):740–753.

Rohlf, F. J.; Slice, D. 1990. Extensions of the Procrustes Method for the Optimal Superimposition of Landmarks. *Systematic Zoology*. 39(1):40–59. DOI: 10.2307/2992207.

Rosas, A.; Pérez-Criado, L.; Bastir, M.; Estalrrich, A.; Huguet, R.; García-Tabernero, A.; Pastor, J. F.; la Rasilla, M. de. 2015. A geometric morphometrics comparative analysis of Neandertal humeri (epiphyses-fused) from the El Sidrón cave site (Asturias, Spain). *Journal of Human Evolution*. 82:51–66. DOI: 10.1016/j.jhevol.2015.02.018.

Saukko, P.; Knight, B. 2004. *Knight's Forensic Pathology*. 3rd ed. London : New York, CRC Press.

Schlager, S. 2015. *Morpho: Calculations and Visualisations Related to Geometric Morphometrics*. Available: http://CRAN.R-project.org/package=Morpho [2015, June 15].

Shakespear, W. [1597] 1993. *Romeo and Juliet*. eBook ed. http://shakespeare.mit.edu/, MIT. (Original work published in 1597).

Shipman, P.; Foster, G.; Schoeninger, M. 1984. Burnt bones and teeth: an experimental study of color, morphology, crystal structure and shrinkage. *Journal of Archaeological Science*. 11(4):307–325. DOI: 10.1016/0305-4403(84)90013-X.

Small, C. G. 1996. *The Statistical Theory of Shape*. (Springer Series in Statistics)New York, Springer.

Spennemann, D. H. R.; Colley, S. M. 1989. Fire in a Pit: the effects of burning on faunal remains. *Archaeozoologia*. 3(1-2):51–64.

Stodden, V. 2015. Reproducing Statistical Results. *Annual Review of Statistics and Its Application*. 2(1):1–19. DOI: 10.1146/annurev-statistics-010814-020127.

Symes, S. A.; L'Abbé, E. N.; Pokines, J. T.; Yuzwa, T.; Messer, D.; Stromquist, A.; Keough, N. 2013. Thermal Alteration to Bone. In *Manual of Forensic Taphonomy*. J.T. Pokines & S.A. Symes, Eds. CRC Press. 367–402.

Symes, S. A.; Rainwater, C. W.; Chapman, E. N.; Gipson, D. R.; Piper, A. L. 2015. 2 - Patterned Thermal Destruction of Human Remains in a Forensic Setting. In *The Analysis of Burned Human Remains*. C.W. Schmidt & S.A. Symes, Eds. San Diego, Academic Press. 17–59.

Tallman, M. 2013. Forelimb to hindlimb shape covariance in extant hominoids and fossil hominins. *Anatomical Record (Hoboken, N.J.: 2007)*. 296(2):290–304. DOI: 10.1002/ar.22624.

Thompson, D. W. [1917] 1992. *On Growth and Form: The Complete Revised Edition*. 2nd ed. New York, Dover Publications. (Original work published in 1917).

Thompson, T. J. U. 2005. Heat-induced dimensional changes in bone and their consequences for forensic anthropology. *Journal of Forensic Sciences*. 50(5):1008–1015.

Thompson, T. J. U. 2009. Burned human remains. In *Handbook of forensic anthropology and archaeology*. USA, Left Coast Press. 295–303.

Thompson, T. J. U.; Gauthier, M.; Islam, M. 2009. The application of a new method of Fourier Transform Infrared Spectroscopy to the analysis of burned bone. *Journal of Archaeological Science*. 36(3):910–914. DOI: 10.1016/j.jas.2008.11.013.

Thurman, M. D.; Willmore, L. J. 1981. A Replicative Cremation Experiment. *North American Archaeologist*. 2(4):275–283. DOI: 10.2190/29A5-84ED-4MB8-EP3M.

Ubelaker, D. H. 2009. The forensic evaluation of burned skeletal remains: a synthesis. *Forensic Science International*. 183(1):1–5.

Van Vark, G. N. 1974. The investigation of human cremated skeletal material by multivariate statistical methods I. Methodology. *Ossa*. 1:63–95.

Van Vark, G. N. 1975. The investigation of human cremated skeletal material by multivariate statistical methods II. Measures. *Ossa*. 2:47–68.

Walker, G. F.; Grainger, R.; Hunter, W. S.; Ledley, R.; Westervelt, F. 1971. New techniques in processing and handling growth data. In *Cranio-facial growth in man*. New York, Pergamon Press. 315–331.

Whyte, T. R. 2001. Distinguishing Remains of Human Cremations from Burned Animal Bones. *Journal of Field Archaeology*. 28(3/4):437–448.

Willey, P. 2014. Stature Estimation. In *Encyclopedia of Global Archaeology*. C. Smith, Ed. Springer New York. 7039–7044.

Zelditch, M. L.; Swiderski, D. L.; Sheets, H. D. 2012. *Geometric Morphometrics for Biologists, A Primer*. 2nd ed. Amsterdam, Academic Press.

6 APPENDIX

6.1 LIST OF ANATOMICAL LANDMARKS OF THE HUMERUS

```
library(knitr)

codebook <- read.csv(file = "./data/codebook.csv", header = TRUE)

kable(codebook)
```

Table 3 - Humeri's landmarks and descriptions adapted from Rosas et al. (2015). Type 3 and other landmarks hard to digitize in a fully computational workstation were not included in our protocol. The last column "Abbreviation" shows the codification of landmarks chosen in the context of this thesis. From the 43 original landmarks, 35 were used in our protocol.

Landmark	Type	Description	Label
1	2	Most projecting point of the lateral epicondyle	S000
2	1	Proximal junction point between lateral epicondyle and *capitulum*	S001
3	1	Distal junction point between lateral epicondyle and *capitulum*	S002
7	2	Proximal junction point between medial *trochlea* and medial epicondyle	S003
8	2	Most projecting point of the medial epicondyle	S004
9	1	Proximal anterior point of the lateral *trochlea*	S005
10	1	Proximal anterior point of the medial *trochlea*	S006
11	1	Proximal posterior point of the lateral *trochlea*	S007
12	1	Proximal posterior point of the medial *trochlea*	S008
13	2	Proximal point of the *olecranon fossa*	S009
14	2	Distal point of the *olecranon fossa*	S010
15	2	Lateral point of the *olecranon fossa*	S011
16	2	Medial point of the *olecranon fossa*	S012
17	2	Maximum curvature between medial epicondyle and shaft	S013
18	2	Most prominent point of the lateral supracondylar ridge	S014
19	1	Proximal point of the lateral supracondylar ridge	S015
20	2	Middle point of the coracobrachial insertion	S016
25	1	Distal point of the greater tubercle crest	S017
26	1	Distal point of the lesser tubercle crest	S018
27	2	Posterior point of the greater tubercle surface	S019
28	2	Lateral point of the greater tubercle surface	S020

Landmark	Type	Description	Label
29	2	Proximal point of the greater tubercle surface	S021
30	2	Medial point of the greater tubercle surface	S022
31	2	Most projected point of the anterior surface of the greater tubercle	S023
32	2	Proximal anterior point where intertubercular groove is between both tubercles	S024
33	2	Most projecting point of the lateral surface of the lesser tubercle	S025
34	2	Proximal point of the lesser tubercle surface	S026
35	2	Anterior point of the lesser tubercle surface	S027
36	2	Distal point of the lesser tubercle surface	S028
37	2	Posterior point of the lesser tubercle surface	S029
38	1	Junction point between the humeral head perimeter and long head of the *biceps brachii*	S030
39	2	Proximal point of the humeral head perimeter	S031
40	2	Posterior point of the humeral head perimeter	S032
41	2	Distal point of the humeral head perimeter	S033
42	2	Anterior point of the humeral head perimeter	S034

In the next page it can be seen where these landmarks are exactly located through a 3D illustration that have been made with the assistance of Landmark Editor.

6.2 VISUAL GUIDE TO THE ANATOMICAL LANDMARKS OF THE HUMERUS

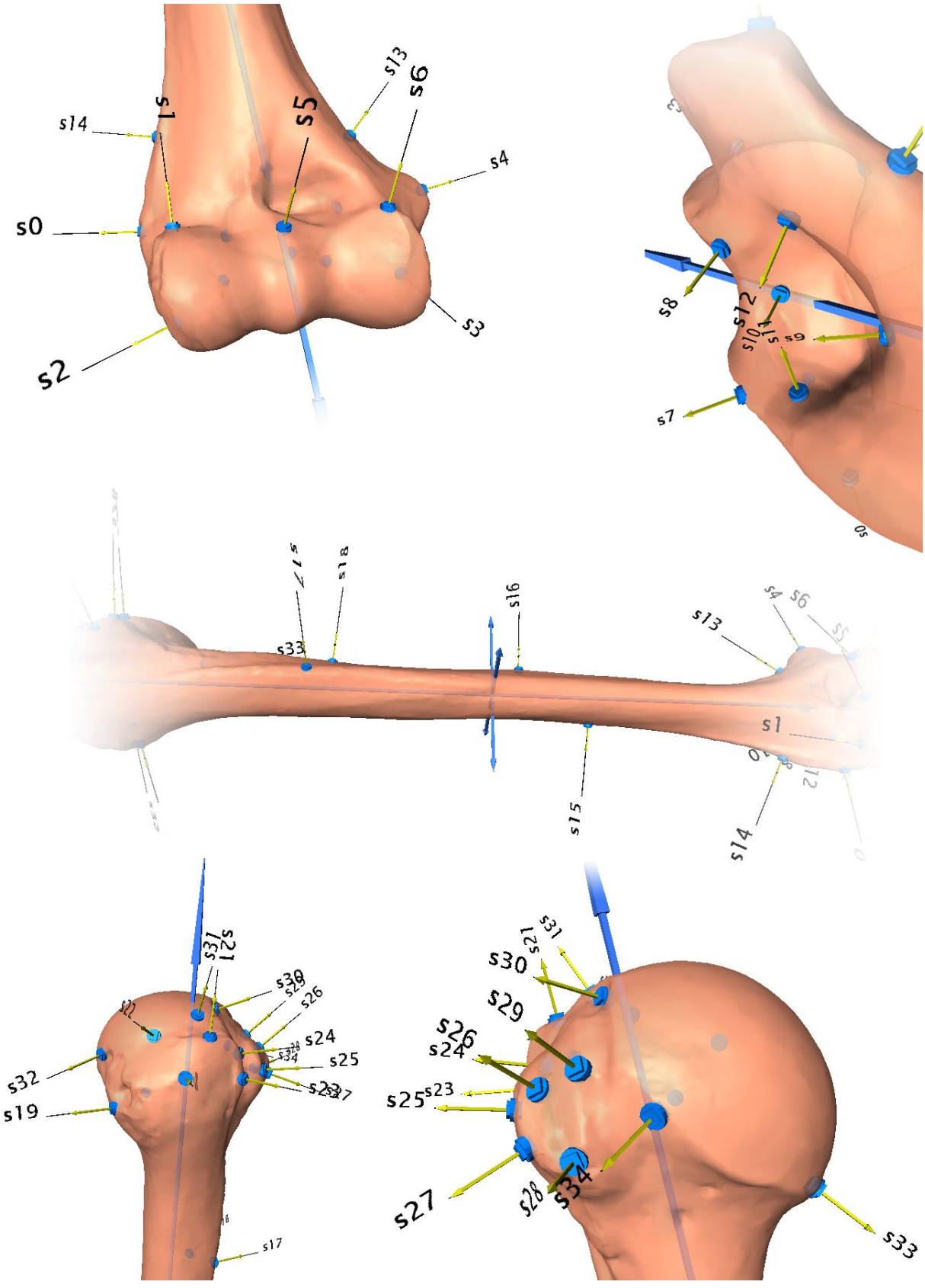

Figure 6-1 - All landmarks from Appendix 6.1 represented on CEI/XXI 51 (unburnt humerus 3D mesh).

6.3 CALCULATION OF FULL PROCRUSTES DISTANCE

```
library(Morpho) # We call this package since it has an useful function
that calculates the complete matrix of Full Procrustes distances

dValue <- regdist(EM, plot = T, rho = "riemdist", dist.mat.out = T) # EM h
as been defined earlier in the Results and Discussion. It's our raw values
 after estimation.missing(), but before gpagen() is applied.

## performing Procrustes Fit in...  0.02876806 secs
## Operation completed in 0.0470929145812988 secs
```

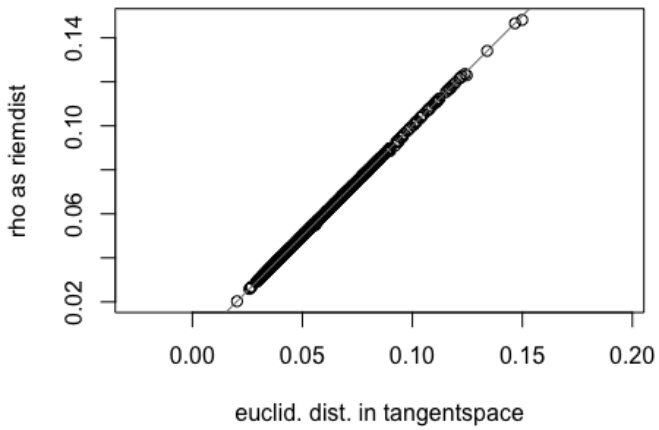

Figure 6-2 - Comparison of Riemannian distance to Euclidean distance in the Tangent Space

```
ProcrustesDistancesMatrix <- as.matrix(dValues$proc.dist)


odd <- seq(1, 37, 2)
even <- seq(2, 38, 2)


index <- matrix(c(odd, even), ncol = 2)


FPD.change <- ProcrustesDistancesMatrix[index] # Our matrix of Procrustes
distances has all the possible values. We have indexed and take the only
19 that really interest us (changes between unburnt and burnt pairs).


dF <- as.vector(matrix(c(rep(0,19), FPD.change), ncol = 19, byrow = T))

# Last lines of code keep it as an attachable variable to our tables. E.g.
 if I desired to attach it to SW, I just need to do:

SW$Df <- Df
```

6.4 QUANTITATIVE VALUES FOR WARPING AND SHRINKING

```
library(knitr)
dt <- read.csv(file = './data/FromGM.csv', header = TRUE)
kable(dt)
```

Table 4 - Tabulated values of Warping and Shrinking. Full Procrustes distances of unburnt-to-burnt were labeled as Warping, and the logarithm of the Centroid Size of the unburnt, minus that of the burnt was labeled as Shrinking. Provided here in case other researchers pretend to use these. In yellow we have a possible case of expansion (i.e. negative shrinking), however CEI/XXI 29 is one of the individuals with virtually mirrored pre-burnt bones, meaning this difference in size can be just due to developmental factors such as fluctuating asymmetry.

ID	Age	Sex	Temperature	Warping	logCS.Before	logCS.After	Shrinking
5	73	F	900	0.0643099	6.658998	6.545755	0.113243
8	83	F	700	0.0477035	6.507733	6.493301	0.014432
17	85	M	900	0.0378350	6.625435	6.503362	0.122073
24	80	F	800	0.0333180	6.690679	6.679033	0.011646
26	90	F	900	0.0392534	6.573471	6.530758	0.042713
29	74	M	800	0.0264085	6.634388	6.647413	-0.013025
32	81	F	800	0.0754552	6.608055	6.434462	0.173593
35	75	M	900	0.0375362	6.602612	6.432676	0.169936
43	70	M	800	0.0202990	6.600072	6.598050	0.002022
49	85	F	850	0.0591030	6.632090	6.504667	0.127423
50	89	F	900	0.0728359	6.542426	6.389417	0.153009
51	70	M	900	0.0709073	6.680793	6.532535	0.148258
53	77	F	800	0.0433352	6.501725	6.354815	0.146910
57	85	M	900	0.0571740	6.588992	6.458196	0.130796
64	87	M	800	0.0324908	6.640177	6.613855	0.026322
65	81	F	900	0.1038588	6.544227	6.385370	0.158857
79	74	M	900	0.0494068	6.675157	6.610388	0.064769
86	78	M	1000	0.0326523	6.684702	6.586534	0.098168
97	88	F	1050	0.0432747	6.611635	6.482052	0.129583

Notice that in the case of CEI/XXI 29, 32, 49, 50, 57, 64 and 65 we couldn't use the pre-burnt 3D mesh, as it has been explained before, and instead mirrored versions of the antimeres were used. Therefore the values for these individuals are possibly the most biased in the sample and should be used with caution.

6.5 R PACKAGES THAT THE CODE DEPENDS ON

Before running any code provided in this thesis, you might need to install packages in R Studio if these were not previously in your computer, to do so, copy paste the following code into your console and run it.

```
# First we make sure to load the required R packages and its dependencies:

if (!require('knitr')){
    install.packages('knitr', dependencies = TRUE)
    library(knitr)
}

if (!require('rmarkdown')){
    install.packages('knitr', dependencies = TRUE)
    library(knitr)
}

options(knitr.table.format = 'markdown')

if (!require('geomorph')){
    install.packages('geomorph', dependencies = TRUE)
    library(geomorph)
}

if (!require('pastecs')){
    install.packages('pastecs', dependencies = TRUE)
    library(pastecs)
}

if (!require('car')){
    install.packages('car', dependencies = TRUE)
    library(pastecs)
}

if (!require('RWeka')){
    install.packages('RWeka', dependencies = TRUE)
    library(RWeka)
}

source('./R/pts2array.R') # gets a function written in collaboration with
David Navega. It reads all .pts files inside a directory into R and saves
them as an array. Used to obtain data from landmark Editor.
```

6.6 THIN-PLATE SPLINE DEFORMATIONS

```
GP <- gridPar(pt.bg = 'black', pt.size = 0.5, n.col.cell = 25) # defines g
eneral graphical proprieties of the following plots.


plotRefToTarget(Shapes[,,1], Shapes[,,2], gridPars = GP, method = 'TPS') #
CEIXXI05F
```

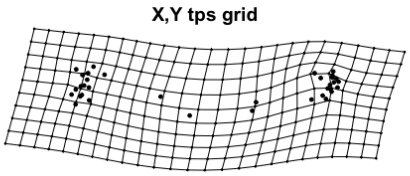

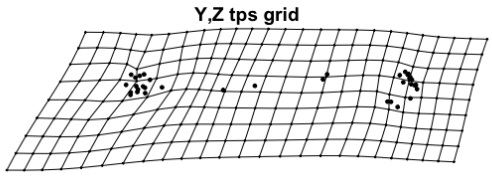


```
plotRefToTarget(Shapes[,,3], Shapes[,,4], gridPars = GP, method = 'TPS') #
CEIXXI08F
```

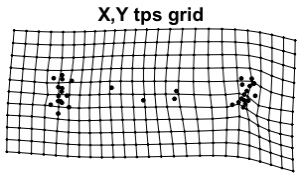

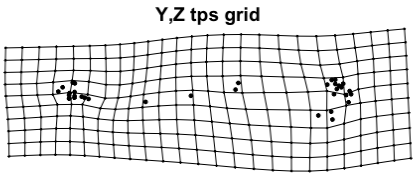


```
plotRefToTarget(Shapes[,,5], Shapes[,,6], gridPars = GP, method = 'TPS') #
CEIXXI17M
```

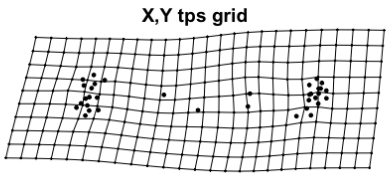

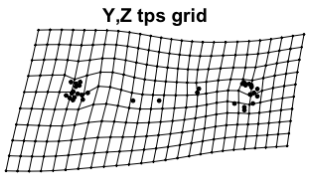


```
plotRefToTarget(Shapes[,,7], Shapes[,,8], gridPars = GP, method = 'TPS') #
CEIXXI24F
```

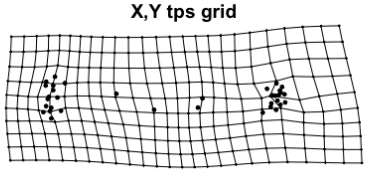

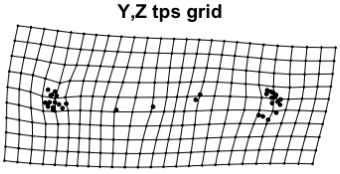

```
plotRefToTarget(Shapes[,,9], Shapes[,,10], gridPars = GP, method = 'TPS')
#CEIXXI26F
```

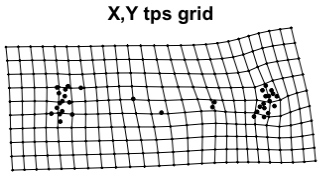

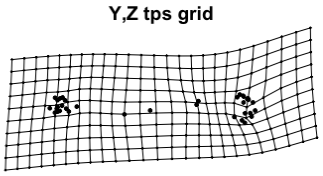


```
plotRefToTarget(Shapes[,,11], Shapes[,,12], gridPars = GP, method = 'TPS')
 #CEIXXI29M
```

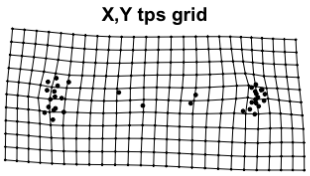

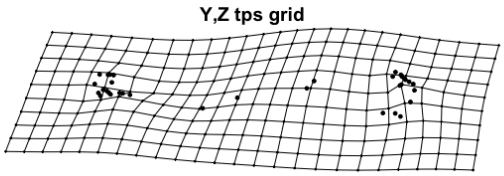


```
plotRefToTarget(Shapes[,,13], Shapes[,,14], gridPars = GP, method = 'TPS')
 #CEIXXI32F
```

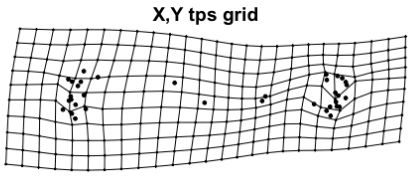

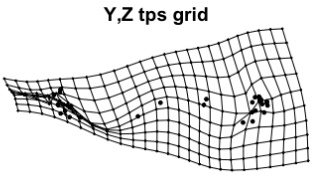


```
plotRefToTarget(Shapes[,,15], Shapes[,,16], gridPars = GP, method = 'TPS')
 #CEIXXI35M
```

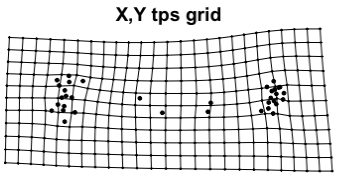

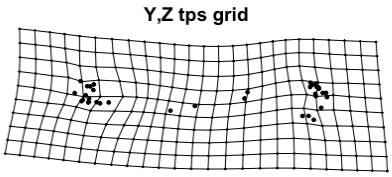


```
plotRefToTarget(Shapes[,,17], Shapes[,,18], gridPars = GP, method = 'TPS')
 #CEIXXI43M
```

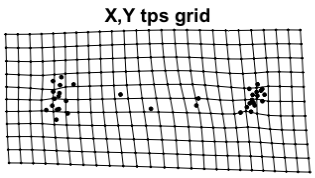

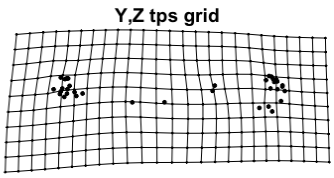

```
plotRefToTarget(Shapes[,,19], Shapes[,,20], gridPars = GP, method = 'TPS')
 #CEIXXI49F
```

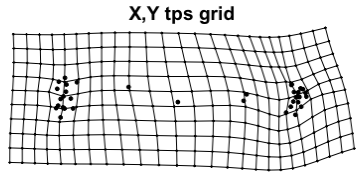

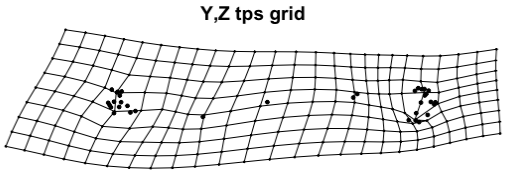


```
plotRefToTarget(Shapes[,,21], Shapes[,,22], gridPars = GP, method = 'TPS')
 #CEIXXI50F
```

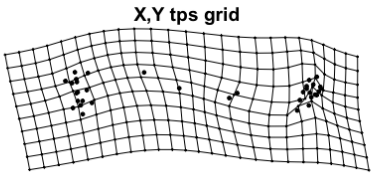

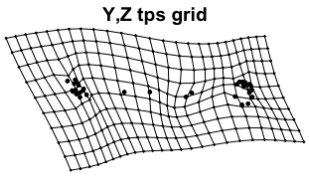


```
plotRefToTarget(Shapes[,,23], Shapes[,,24], gridPars = GP, method = 'TPS')
 #CEIXXI51M
```

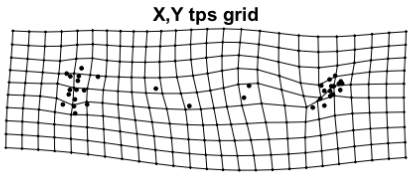

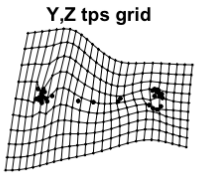


```
plotRefToTarget(Shapes[,,25], Shapes[,,26], gridPars = GP, method = 'TPS')
 #CEIXXI53F
```

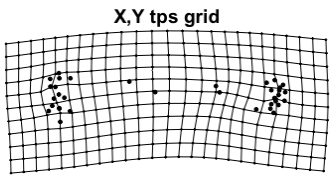

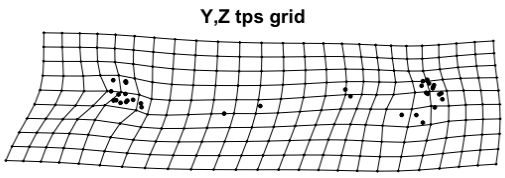


```
plotRefToTarget(Shapes[,,27], Shapes[,,28], gridPars = GP, method = 'TPS')
 #CEIXXI57M
```

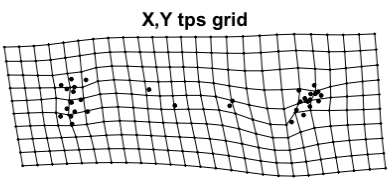

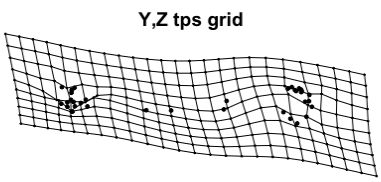

```
plotRefToTarget(Shapes[,,29], Shapes[,,30], gridPars = GP, method = 'TPS')
 #CEIXXI64M
```

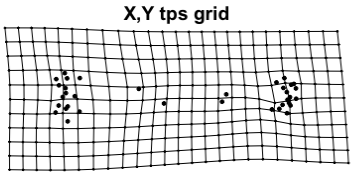

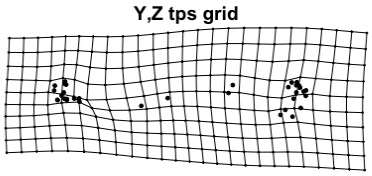


```
plotRefToTarget(Shapes[,,31], Shapes[,,32], gridPars = GP, method = 'TPS')
 #CEIXXI65F
```

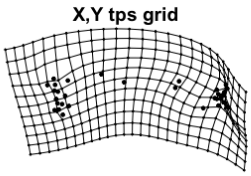

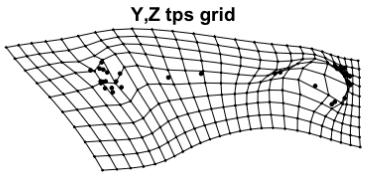


```
plotRefToTarget(Shapes[,,33], Shapes[,,34], gridPars = GP, method = 'TPS')
 #CEIXXI79M
```

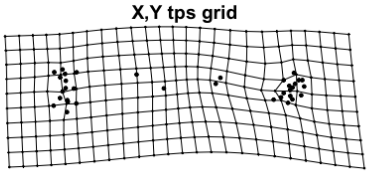

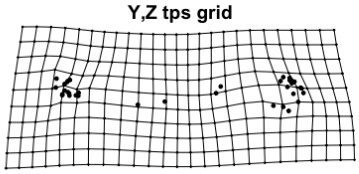


```
plotRefToTarget(Shapes[,,35], Shapes[,,36], gridPars = GP, method = 'TPS')
 #CEIXXI86M
```

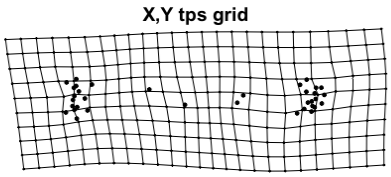

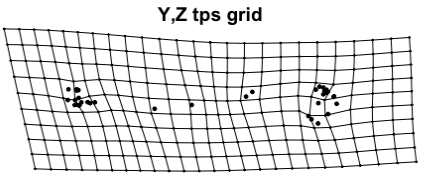


```
plotRefToTarget(Shapes[,,37], Shapes[,,38], gridPars = GP, method = 'TPS')
 #CEIXXI97F
```

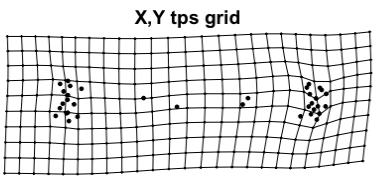

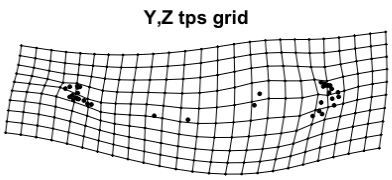

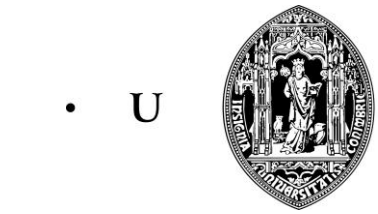
· U
C ·